Research Article

Muhammad Jawad Munawar, Chengyan Lin*, Dong Chunmei, Xianguo Zhang, Haiyan Zhao, Shuming Xiao, Tahir Azeem, Muhammad Aleem Zahid, and Cunfei Ma

Architecture and reservoir quality of low-permeable Eocene lacustrine turbidite sandstone from the Dongying Depression, East China

https://doi.org/10.1515/geo-2018-0008
Received Jan 26, 2018; accepted Mar 13, 2018

Abstract: The architecture and quality of lacustrine turbidites that act as petroleum reservoirs are less well documented. Reservoir architecture and multiscale heterogeneity in turbidites represent serious challenges to production performance. Additionally, establishing a hierarchy profile to delineate heterogeneity is a challenging task in lacustrine turbidite deposits. Here, we report on the turbidites in the middle third member of the Eocene Shahejie Formation (Es3), which was deposited during extensive Middle to Late Eocene rifting in the Dongying Depression. Seismic records, wireline log responses, and core observations were integrated to describe the reservoir heterogeneity by delineating the architectural elements, sequence stratigraphic framework and lithofacies assemblage. A petrographic approach was adopted to constrain microscopic heterogeneity using an optical microscope, routine core analyses and X-ray diffraction (XRD) analyses. The Es3m member is interpreted as a sequence set composed of four composite sequences: CS1, CS2, CS3 and CS4. A total of forty-five sequences were identified within these four composite sequences. Sand bodies were mainly deposited as channels, levees, overbank splays, lobes and lobe fringes. The combination of fining-upward and coarsening-upward lithofacies patterns in the architectural elements produces highly complex composite flow units. Microscopic heterogeneity is produced by diagenetic alteration processes (*i.e.*, feldspar dissolution, authigenic clay formation and quartz cementation). The widespread kaolinization of feldspar and mobilization of materials enhanced the quality of the reservoir by producing secondary enlarged pores. In contrast, the formation of pore-filling authigenic illite and illite/smectite clays reduced its permeability. Recovery rates are higher in the axial areas and smaller in the marginal areas of architectural elements. This study represents a significant insight into the reservoir architecture and heterogeneity of lacustrine turbidites, and the understanding of compartmentalization and distribution of high-quality sand reservoirs can be applied to improve primary and secondary production in these fields.

Keywords: Deep water; Architectural Elements; Lacustrine Turbidite; Sequence Stratigraphy; Reservoir Quality; Turbidite Lithofacies; Dongying Depression

***Corresponding Author: Chengyan Lin:** School of Geosciences, China University of Petroleum (Qingdao), P.R China, 266580; Key laboratory of reservoir Geology in Shandong Province, Qingdao, P.R China, 266580; Email: ycdzycms2017@126.com
Muhammad Jawad Munawar, Xianguo Zhang, Cunfei Ma: School of Geosciences, China University of Petroleum (Qingdao), P.R China, 266580
Dong Chunmei: School of Geosciences, China University of Petroleum (Qingdao), P.R China, 266580; Key laboratory of reservoir Geology in Shandong Province, Qingdao, P.R China, 266580
Haiyan Zhao, Shuming Xiao: Xianhe Oil Production Plant, Shengli Oil Field, SinoPec
Tahir Azeem: Department of Earth Sciences, Quaid-I-Azam University, Islamabad, Pakistan
Muhammad Aleem Zahid: Faculty of Marine Sciences, Lasbela University, Uthal, Balochistan, Pakistan, 90250

1 Introduction

Deep-water turbidite sandstones are commonly regarded to be good petroleum reservoirs [4, 7, 23, 43, 44, 57, 70, 71]. Understanding the heterogeneity in these reservoirs is crucial for petroleum exploration and production [4, 43, 44, 82]. Heterogeneity occurs across different scales and is influenced by both depositional and diagenetic processes [46, 53, 88, 89]. To understand reservoir heterogeneity, it is necessary to comprehensively characterize the reservoir in order to observe the processes and factors that influence reservoir producibility. Reservoir architec-

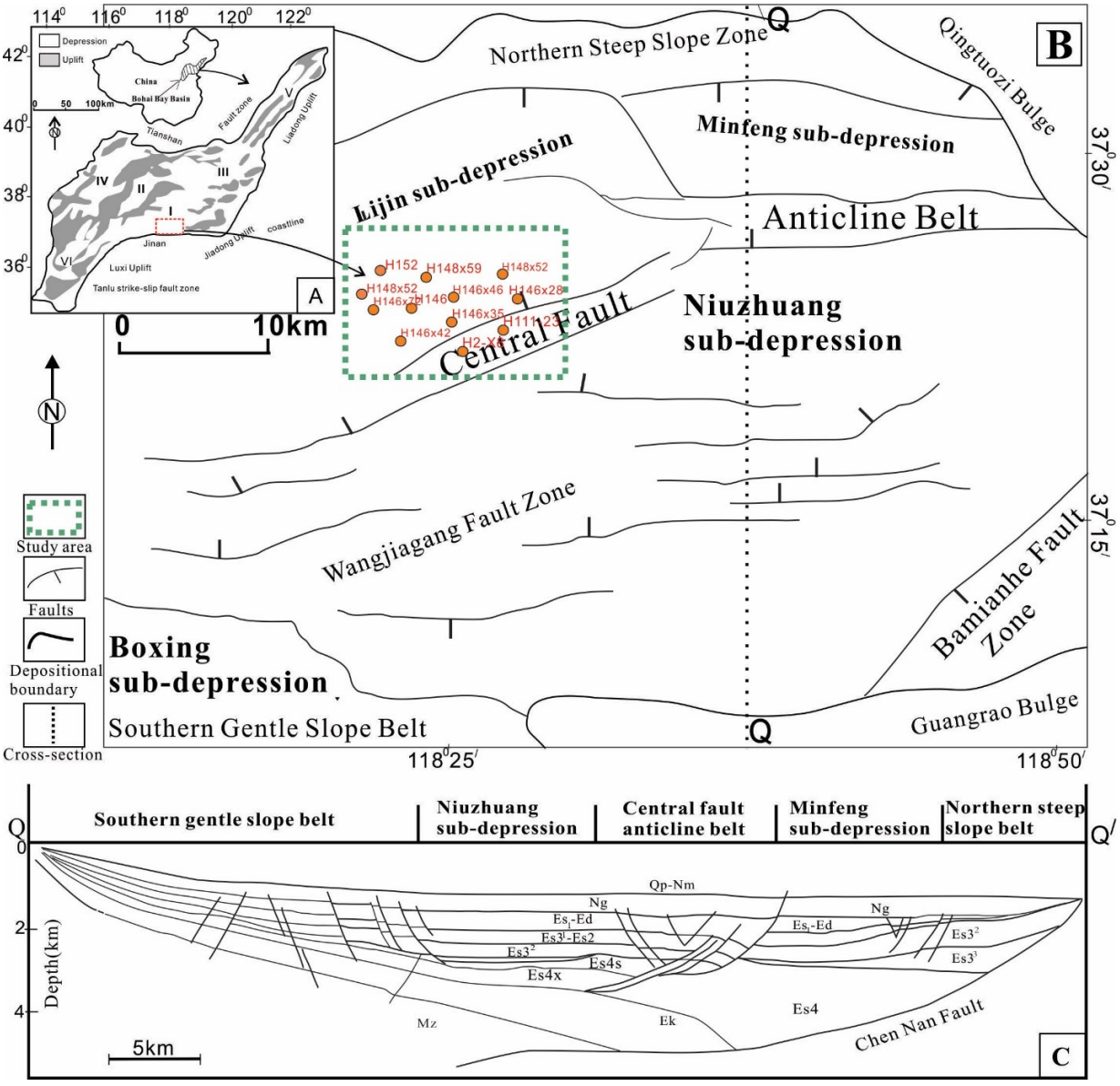

Figure 1: (A) Index map showing Bohai Bay Basin and its subtectonic units; (I) Jiyang subbasin, (II) Huanghua subbasin, (III) Bozhong subbasin, (IV) Zhezhong subbasin, (V) Liaohe subbasin (VI) Dongpu subbasin; (B) structural map showing study area in Dongying Depression (C) Cross-section through Dongying Depression showing key stratigraphic intervals and tectonic features. Note: Location of cross-section is marked by Q-Q/ in "B". (modified from [25].

ture exerts a major control on primary and secondary production. The concept of elements was first introduced by Mutti and Normark [50] for a deep-water turbidite system. In turbidite systems, the elements represent only large-scale features, such as channels, lobes and overbank deposits. The architectural elements can be identified based on facies assemblage and depositional geometry. [48] proposed two interrelated ideas to understand architectural complexities in fluvial systems. The first concept was related to lithofacies assemblages over a wide range of physical scales (*i.e.*, from ripple laminations to an entire depositional system). The second concept addresses architectural elements, which are sets of lithologies that are characterized by their geometries, scales and depositional processes. [48] observed some similarities in fluvial deposits and coarse-grained submarine-fan deposits, particularly the channel fills. He suggested that it is possible to establish an architectural hierarchy in turbidite environments. [14] took up these ideas and provided numerous illustrations of modern and ancient deep-marine channel systems.

Table 1: Recognition criteria of architectural elements from log motifs.

Architectural elements	Lithology and Log Motifs	SP log shape
Lobe	Massive sandstone with interbedded siltstone, high amplitude funnel shape SP curve, thickness 1.5-6m	
Lobe Fringe	Siltstone, silty mudstone, low amplitude funnel-shaped SP curve, thickness 0.5-2m	
Channel	Massive sandstone and sandstone with large clasts, High amplitude serrated bell shaped SP curve, thickness 2 m-6 m,	
Levee	Siltstone and silty mudstone, low amplitude serrated bell-shaped SP curve bell-shaped, thick 0.5 m-2 m	
Overbank Splay	Thin massive sandstone to fine silty mudstone, potential curve high to low amplitude funnel-shaped SP curve, thickness 0.5 m-3 m	

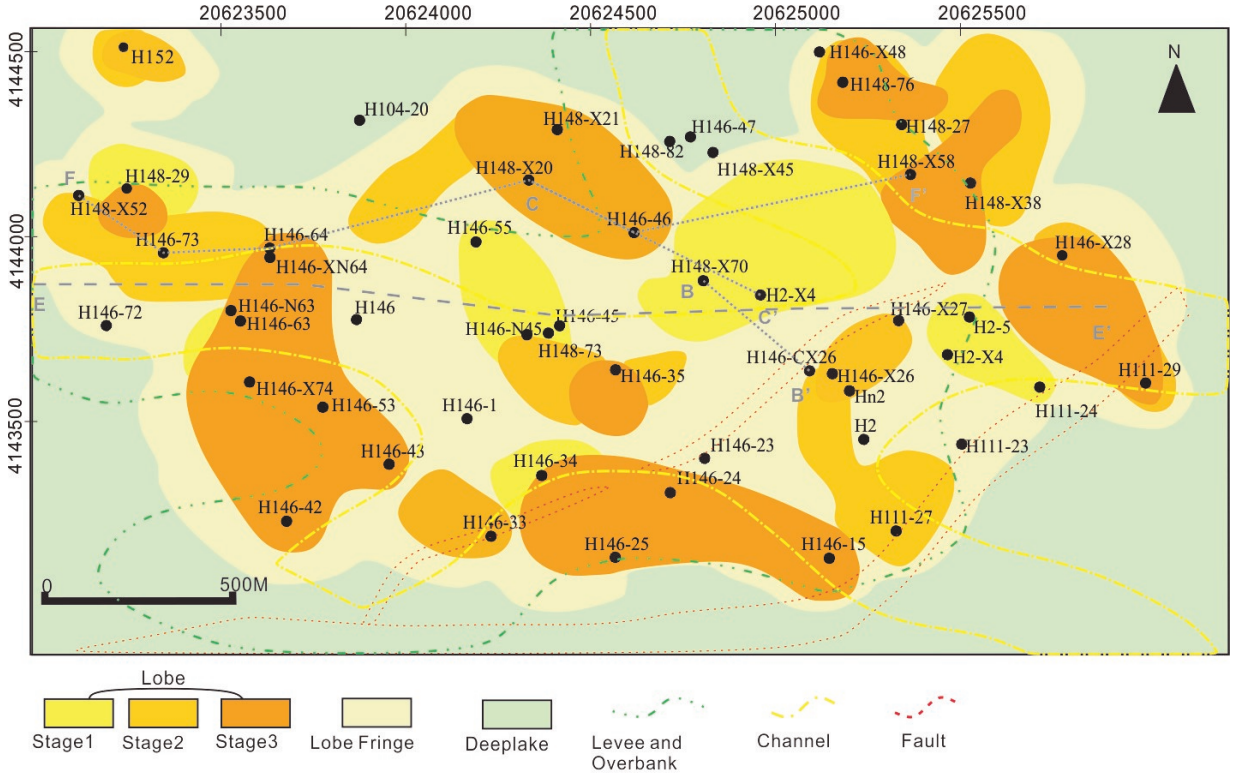

Figure 2: Generalized map of architectural elements of Es3m interval. Map is showing locations of well cross-sections and seismic-sections used in this paper. B-B', C-C' (Figure 9) and F-F' (Figure 13) are well cross-sections; while E-E' is seismic-section (Figure 11). This depositional model is based on spatial and temporal information inferred and gathered from different data sets of study area.

Reservoir architecture exerts a primary control on the primary and secondary production. Four main types of heterogeneity occur in petroleum reservoirs, namely, microscopic, mesoscopic, macroscopic and megascopic heterogeneities [82]. Understanding the reservoir heterogeneity depends on characterization of the architectural elements, which is a key to improving primary and secondary production. In this study, we examined the middle third member of the Eocene Shahejie Formation (Es3m), which is a major reservoir interval in its basin. The Es3m sandstones were deposited as turbidites in a lacustrine basin [31]. We studied their lithofacies assemblages, reservoir architecture and petrographic characteristics to distinguish potentially high-quality reservoir units that may yield primary and enhanced secondary production.

2 Geological setting

The Bohai Bay Basin is considered one of the most significant oil-producing provinces in East China. The Jiyang Subbasin is one of the six major subbasins within the Bohai Bay Basin [26, 36]. The Dongying Depression is located in the southeastern region of the Jiyang Subbasin (Figure 1). The Dongying Depression contains a complete petroleum system with a source, seals and reservoirs [54, 90]. Figure 2 shows the depositional pattern and distribution of the channel, lobe and overbank elements in the study area. The evolutionary history of the system indicates that it is an asymmetrical complex rift basin that developed from the Late Jurassic through the Early Cenozoic [30, 86]. The Dongying Depression is a typical half-graben faulted basin that is surrounded by uplifts on four sides. The anticline belt in this extensional system is due to roll-over folding [22]. The depositional history of the depression has mainly been influenced by the growth of normal faults, which extend into the basement and represent primary controls on the distribution of Cenozoic sediments [22, 25, 37]. The multiple uplifts provided multiple provenances for the sediments in the basin [37]. Therefore, large amounts of detrital material were transported into the basin and formed sedimentary facies of deltas and turbidite fans [12, 31, 37]. The deposition of turbidite sandstones occurred largely along an E–W axis and on the southern slope of the basin [12]. However, small-scale fan deltas and alluvial fans were deposited in lakeshore and shallow lake environments on the northern slope [31, 37]. Several authors have provided detailed descriptions of the Paleogene stratigraphy [26, 92] in the Jiyang Subbasin. In this subbasin, the Paleogene succession is more than 7000 m thick, and the Neogene succession is 1000-2000 m thick. The entire Cenozoic succession is dominated by non-marine sandstones and mudrocks with minor carbonates and evaporites. The objective of this study, the Es3 member, ranges in thickness from 700 to 1,200 m and generally contains lacustrine oil shale that accumulated rapidly, as well as dark gray mudstones, calcareous mudstones and sandstones [34] (Figure 3).

3 Materials & methods

A total of fifty-eight wells with wireline logs and six wells with cores were analyzed in this study. Core logging was used to identify sedimentary structures and define sedimentary facies. Core observations were calibrated to wireline logs; similarly, wireline logs were correlated with seismic data to enable the mapping of architectural elements and sequence boundaries. Architectural elements were first identified in individual wells based on geomorphic and geometrical features and on depositional processes inferred from sedimentary structures in well cores. These elements were then mapped and correlated in uncored wells based on their corresponding log motifs (Table 1). Cross-sections oriented parallel and perpendicular to the depositional dip and plan-view architectural maps were constructed in order to determine the distribution patterns of the architectural elements. A hierarchy scheme proposed by Sprague *et al.* [77] was adopted to establish the physical stratigraphy. Individual sequences are identified as LST sandstone capped by HST or TST hemiplegic mudstone. Sequences are bundled into composite sequences and composite sequences are bundled into composite sequence sets based on the physical thickness of the sequence boundary (mudstone) dividing these units. The sequence boundary identification criterion is taken from Sprague *et al.* [77].

An optical polarizing microscope (ZEISS AXIO, Imager A2m) in transmission mode was used to document the whole-rock mineralogy, diagenetic relationships, porosity characteristics and clay occurrences in the pores of these samples [6, 28, 65]. Thin sections of all samples were prepared by saturating and impregnating them with blue epoxy resin. The same thin sections were analyzed using a scanning electron microscope (SEM). A Philips-FEI Quanta 200 SEM at the Shingli Oil field research labs in Dongying was used in this study. Small unpolished rock sample fragments were mounted on a stage in the vacuum chamber of the SEM, and a voltage of 20 kV was used for SEM imaging. The X-ray diffraction (XRD) analysis of

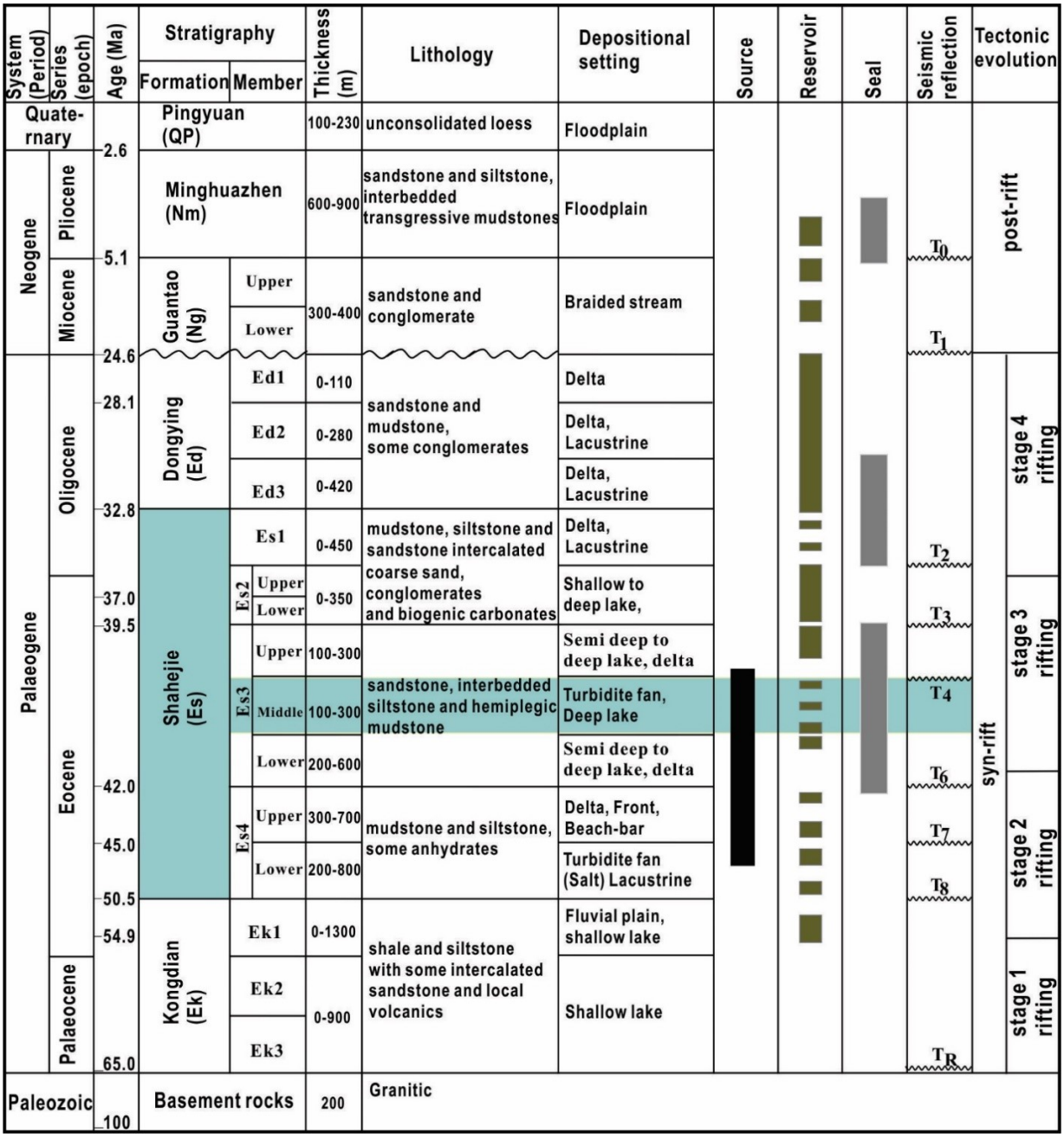

Figure 3: Generalized stratigraphic chart showing Cenozoic-Quaternary sequence with tectonic evolution and petroleum play in the Dongying Depression, Bohai, Bay Basin, East China. (modified from [25]).

minerals was performed using a D500 X-ray diffractometer with Ni-filtered Cu-Ka radiation to qualitatively determine the whole-rock mineralogy and the clay mineralogical content. These samples were prepared and analyzed in the petrographic laboratories at the School of Geosciences, China University of Petroleum (East China).

4 Results

4.1 Lithofacies

Middleton and Hampton [52] suggested that sedimentary structures can be used to define their depositional processes but cannot be used to infer their transport mechanisms. Transport processes can be inferred once a depositional mechanism is established. We thus characterized

the depositional mechanism of each facies. Three potential depositional processes are interpreted in these samples: (1) debris flows; (2) turbidity currents; and (3) cogenetic flows.

4.1.1 Lithofacies 1 (Massive sandstones)

Massive sandstones occur in very thick beds and represent the most abundant lithofacies in the study area. These units comprise structureless light gray sand and are mostly oil-stained, with no evident sedimentary structures (Figure 4A, B). The sandstone is moderately to well sorted, and its grain size ranges from fine to medium sand. The thicknesses of the beds range from 10 cm to 100 cm. These sandstones mostly grade upwards into parallel or convolute laminated facies. Massive sandstone facies exhibit sharp, loaded or erosional bases. Water-escape structures (Figure 5) are recognizable in some of these sandstones. These dewatered sandstones are injected into overlying and underlying facies.

These structureless sandstones are considered to represent the Ta division of a Bouma sequence. They mostly occur in the axial areas of channels, lobes, overbank splays, and occasionally thin sheet sands [29, 43, 57]. Shanmugam [70] suggested a debris flow mechanism for these structureless sandstone deposits. The presence of dewatered sandstone and associated sand injections indicates that these sandstones were deposited with excess intergranular water. Therefore, they are interpreted to represent the products of high- and low-density turbidity currents [16, 27].

4.1.2 Lithofacies 2 (Mudclast-rich, muddy sandstone)

This lithofacies comprises light gray to gray fine-grained muddy sandstone or mudclast-rich siltstone. These facies contain large (1-5 cm) mudclasts that float within a muddy-silty matrix (Figure 4D, E). Small quantities of very coarse-grained sand are also present in association with mudclasts that have been incorporated by injection (Figure 4E). As they are larger than the core diameter, these clasts extend beyond the dimensions of the drill core. If original lamination is present, it is sometimes folded around the clasts (Figure 6), and the edges of the clasts are abraded by matrix sand. The thicknesses of the beds range from 5 cm to 1 m.

Most of the contorted facies mainly occur in channels and comprise slumps and debris flows [43]. The presence of floating clasts and the fact that the major axes of these clasts are oriented in the flow direction are indicative of a sheared debris flow [70]. The ubiquity of the large clasts and the injection of coarse-grained sand into the muddy-silty matrix by folding are also indicative of a debris flow [17]. Soft-sediment deformation features occur and were caused by the fluidization of the sediments, which may have been caused by seismic activity. These facies are thus interpreted to have been deposited by debris flows.

4.1.3 Lithofacies 3 (Carbonaceous clast-rich sandstone)

This unit comprises light gray argillaceous fine-grained sandstone with floating dark gray to black carbonaceous debris clasts that are 1-2 cm in diameter (Figure 4C, 6). These rocks appear to be cleaner and contain less mud than lithofacies 2. These rocks also exhibit much less chaotic fabrics due to their much lower quantities of mudclasts. Usually, this facies co-exists with and overlies the mudclast-rich facies; it also sometimes grades upward into massive sandstone.

Carbonaceous debris is an indicator of a fluvio-deltaic sediment source. Carbonaceous material can be transported to the upper slope by shelf floods [67]. In channel complexes, extensive mudclasts occur at the bases of channels and are overlain by sandy beds and carbonaceous material. The proportions of mudclasts decrease towards the top [27, 43]. These facies are thus interpreted to represent the depositional product of channelized turbidity currents.

4.1.4 Lithofacies 4 (Laminated fine-grained sandstone or siltstone)

In this lithofacies, fine-grained sandstones and siltstones are laminated with dark gray or reddish mud layers (Figure 6). Usually, the sand laminae have erosive bases that cut into the underlying mud laminae. Convolute lamination also occurs with folded and inclined imbricated laminae forming duplex-like structures (Figure 4G, H). The contorted units are bounded by horizontal, undeformed and parallel laminae. Sometimes these convolute laminae are found within the substrate. The thicknesses of these beds range from a few cm to 1-2 m. The thicknesses of individual mud laminae range from 1 mm to 1 cm.

The parallel laminated units are considered to represent the Tb division of a Bouma sequence, whereas the convolute bedding is interpreted to represent the Tc division of a Bouma sequence. Shanmugam [71] suggested a

Figure 4: Figure shows different lithofacies with their diagnostic features. (A) and (B) are massive sandstone facies (lithofacies 1); (C) Carbonaceous clast rich sandstone (lithofacies 3) grading into massive sandstone (lithofacies 1); (D) and (E) showing large clasts are floating in muddy sandy matrix, clasts are abraded by surrounding sandy matrix (Black arrows) (lithofacies 2); (F) \Showing parallel lamination, where fine sandstone or siltstone is laminated with gray mud (lithofacies 4); while in the middle is massive dark gray to black hemiplegic mudstone; (G) and (H) inclined imbricated laminae forming duplex-like structures.

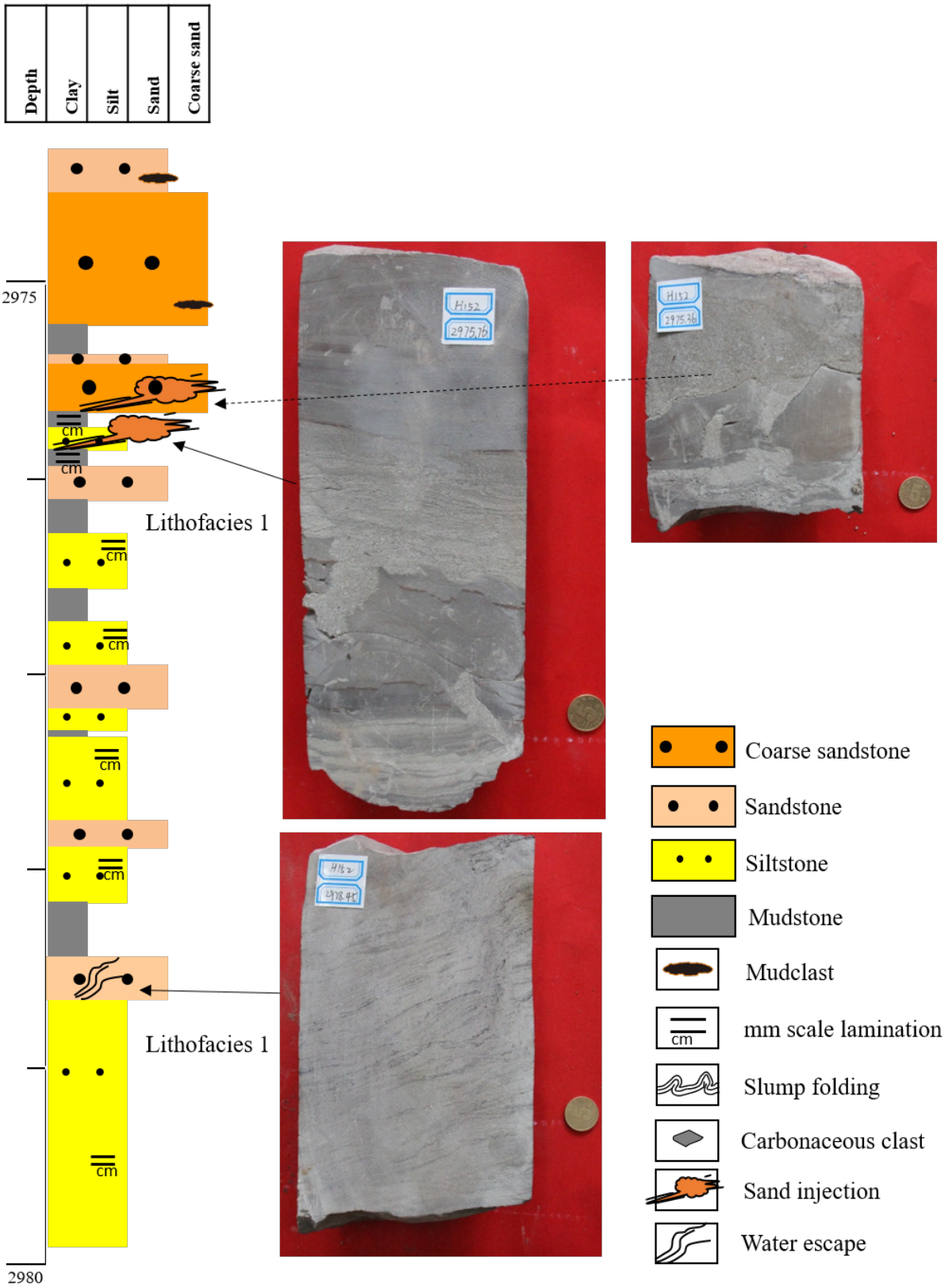

Figure 5: Core log from Well H152 showing sand injections and water escape structure in lithofacies 1. Note; Dewatered sandstone, shows water escape structure with wispy dark layers.

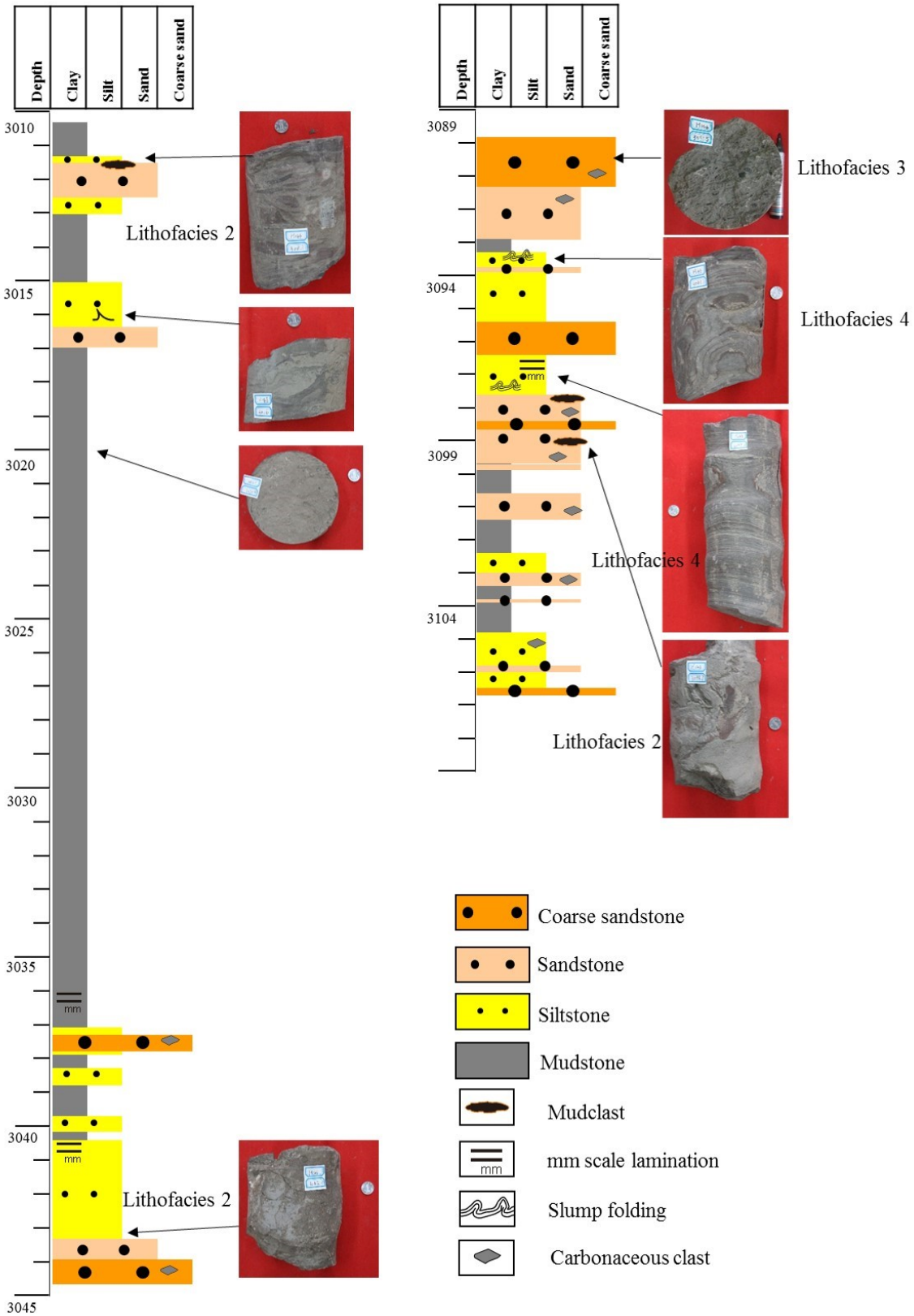

Figure 6: Core log from Well H146 showing mudclast in lithofacies 2, carbonaceous clast in lithofacies 3 and lamination and slump folding in lithofacies 4.

bottom-current reworking origin for the parallel lamination. Based on a coherent structure model, Allen [1] proposed that parallel laminations are developed from upper-stage plane beds by turbulent currents. Eggenhuisen [17] also inferred these facies to be upper-stage plane bed laminations. Convolute laminae developed due to the disaggregation of aggrading beds caused by dewatering and shear by the overriding flow [17]. These facies are interpreted to be the product of low-density turbidites [27, 27]

4.1.5 Lithofacies 5 (Hemipelagic mudstone)

Two types of hemipelagic mudstone occur in the study area: (1) reddish mudstone and (2) dark gray to black mudstone. The reddish mudstone occurs as thin laminae (1 cm) in thin-bedded turbidites (Figure 6), and the dark gray to black mudstone occurs as thin laminae (<1 cm) (Figure 7) and thick beds that can reach thicknesses of up to 10 m. Thin laminae of hemipelagic siltstone sometimes occur between these beds. Thick beds of hemipelagic mudstone can be correlated between wells and can also be traced using seismic data.

Hemipelagic mud is considered to represent the Te division of a Bouma sequence. The reddish mudstone contains hematite, which formed under oxic seafloor conditions [85]. In contrast, the dark gray mudstone formed under anoxic seafloor conditions. Both of these are interpreted to reflect the hemipelagic settling of mud and silt.

4.2 Architectural elements

The architectural elements in this region exhibit definite lateral and vertical arrangements of lithofacies, geometries and geomorphologies. The stratigraphic relationships between architectural elements indicate that the sediments of Es3m were deposited in a complex system of channels, levees, overbank splays, lobes and lobe fringes.

4.2.1 Channels

Channels are only present in the lower part of the Es3m sequence. They are 2 m to 6 m thick and 380 m to 1200 m wide. Most of them have erosive bases and contain lithofacies 1 and lithofacies 2, which features large mudclasts floating in a finer sand matrix (Figure 8A, C). The entrainment of such large particles indicates the flow strength of these channels. Basically, these channels are composed of discrete amalgamated units that are separated by thin erosive surfaces. Debris flow processes are interpreted to be dominant at the channel base and eroded the channel bases and sidewalls. Generally, clast-rich debris flow facies containing intervals of massive coarse sand are present at the bottom and are overlain by laminated facies. At the top, these elements are preserved by a relatively horizontal mud layer exhibiting an overall fining upward trend.

4.2.2 Levees

Levees are composed of fine-grained lithofacies 4 and flank both sides of the channels. They represent the wedge-shaped elevated margins of the channels, with thicknesses ranging from 0.5 m to 2 m. They are thicker near the channel margins and laterally thin outward (Figure 8A, C). They are typically composed of thin-bedded laminated siltstone. These siltstones represent the upper parts of turbidity flows, which are not totally confined by the channels. Low-density flows usually feed fine-grained sediments to overbank areas. The upper parts of turbidity flows can be interpreted as low-density turbidity flows, as reflected by the nature of the traction and suspension of their depositional mechanism.

4.2.3 Overbank splays

Overbank splays are present where levee banks are breached. These deposits dominantly comprise lithofacies 2 and range in thickness from 0.5 m to 3 m. Overbank splay sediments are mostly deposited in a contrasting manner as levees; as the thickness of a levee decreases moving away from the channel margins, the thickness of the splay increases. Splays are present where a channel bifurcates or changes its angle. When a flow passes through the splay, its velocity suddenly decreases and its sediment load is deposited rapidly. This rapid deposition results in a bifurcating channel pattern.

4.2.4 Lobes

Lobes are thick stacked lenticular bodies that are superimposed on the channel complexes in the study area. They record maximum thicknesses of 6 m near their axes and minimum thicknesses of 1.5 m near their margins. Generally, lobes are composed of lithofacies 1, lithofacies 3 and lithofacies 4 at their bases and exhibit an overall coarsening-upward trend. Moving outward towards the

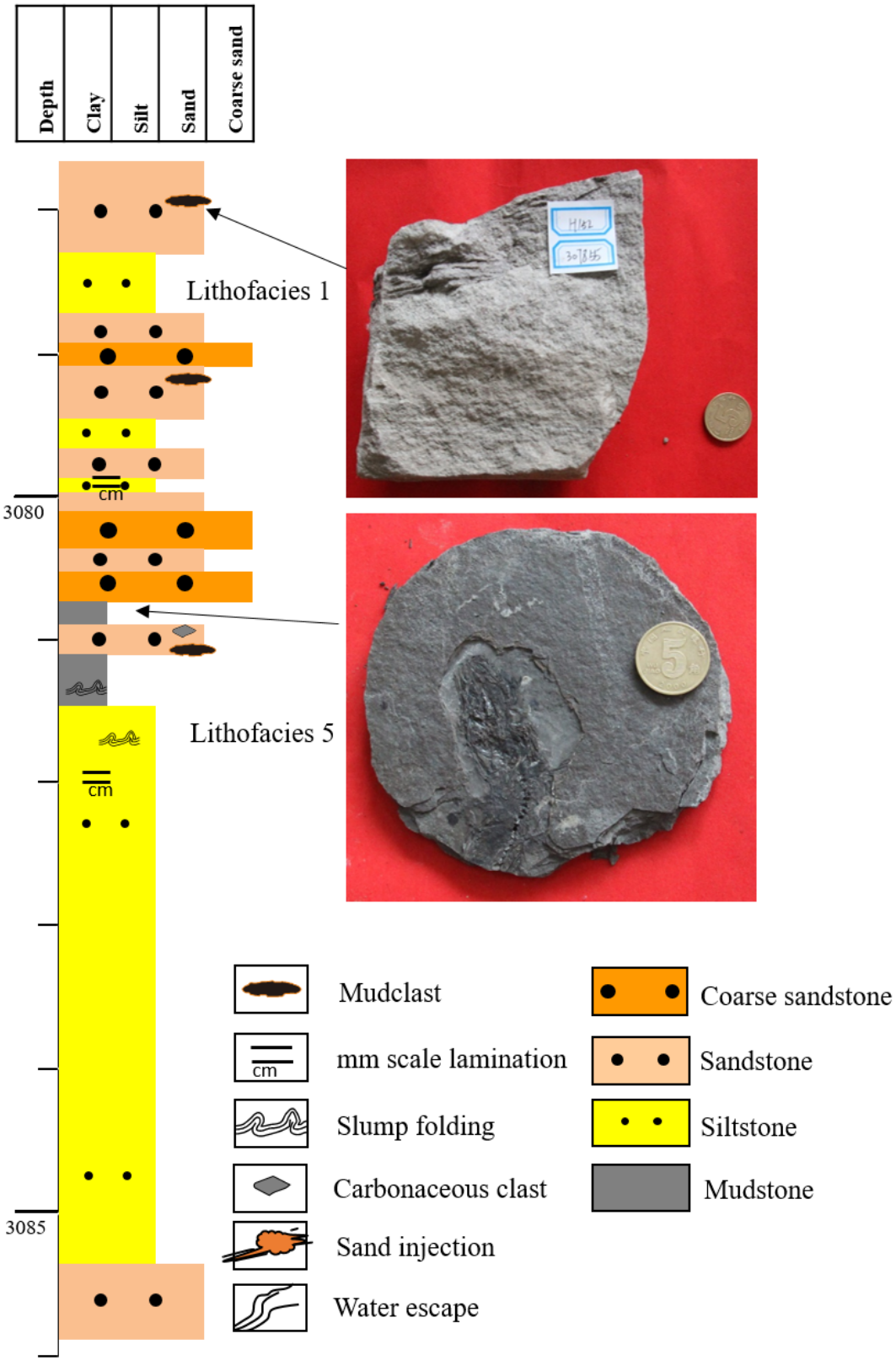

Figure 7: Core log from Well H152 showing mudclast in lithofacies 1 and dark grey hemiplegic mudstone in lithofacies 5.

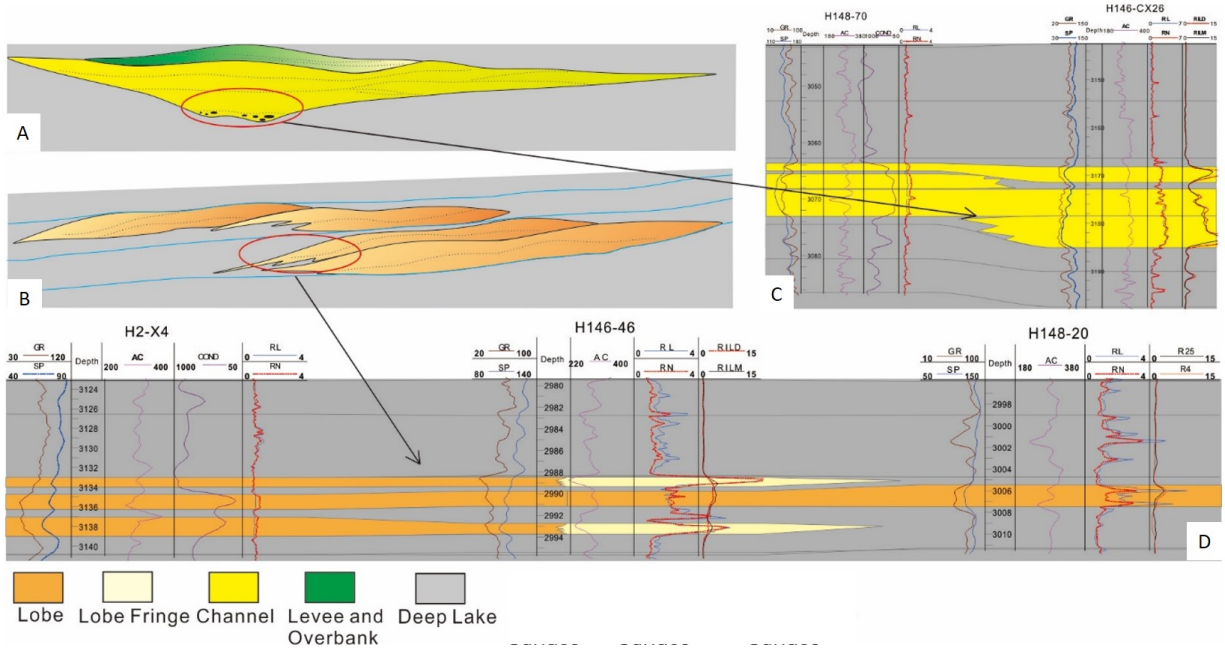

Figure 8: (A) depositional model of channel; (B) depositional model of lobe; (C) representation of channel from well correlation; (D) representation of Lobe.

lobe fringes, the proportion of framework grains decreases and that of the fine-grained matrix increases. Lobes do not exhibit erosive bases due to the low velocity of the flow during deposition. They are interpreted to occur at the mouths of channels where the channel is no longer confined by a levee. At this stage, the flow spreads out, the velocity rapidly decreases, and thick lobe-shaped bodies of sediment are deposited.

4.2.5 Lobe Fringes

Lobe fringes comprise thin deposits of graded lithofacies 2. These lobe fringes are typically 0.5 m to 3 m thick, and they are characterized by thin separations of fine siltstone. Lobe fringes continually shift during the development of lobes, thus causing fine siltstone to be variably distributed within the lobe body (Figure 8B, D).

4.3 Architectural hierarchy

Individual elements, such as channel elements, lobe elements, levees and overbank splays, are bounded by hemipelagic siltstone or mud. These are equivalent to the fourth-order surfaces of *Miall*. Their top surfaces are defined by relatively horizontal hemipelagic mud beds, while their bases represent concave-up in channel elements. These surfaces can be identified in cores with meter-scale mud beds and relatively low gamma ray (GR) values (Figure 9A, B, C).

The channel and lobe elements are bounded by surfaces that are equivalent to the fifth-order surfaces of *Miall*. The top bounding surfaces are mostly flat, whereas their basal surfaces are slightly concave upward. These units are marked by high-frequency changes in deposition and erosion. These surfaces are characterized by a relatively thick layer of hemipelagic mud with low GR values and high AC log motifs (Figure 9A, B, C). In seismic profiles, these surfaces develop a weak impedance contrast that is recognizable by its weak reflectance (Figure 10).

Channel and lobe complexes represent short-term sea level changes and tectonic activities. They are equivalent to the “third-order” turbidite stage of Mutti and Normark [56]. Thick beds of hemipelagic mud reflect a very low to absent sand supply to deep-water settings [19, 77]. These hemipelagic intervals can be used to map these surfaces and determine the number of cycles in basinal studies. Seismic sedimentology is a promising frontier and have great potential in reservoir deposition research [93, 94]. The bounding surfaces can be recognized in seismic profiles based on their strong reflectance (Figure 10), and they can be mapped throughout well-sparse areas.

Individual depositional systems, which are composed of multiple composite channel/lobe complexes are bounded by thick hemipelagic mudstones that represent

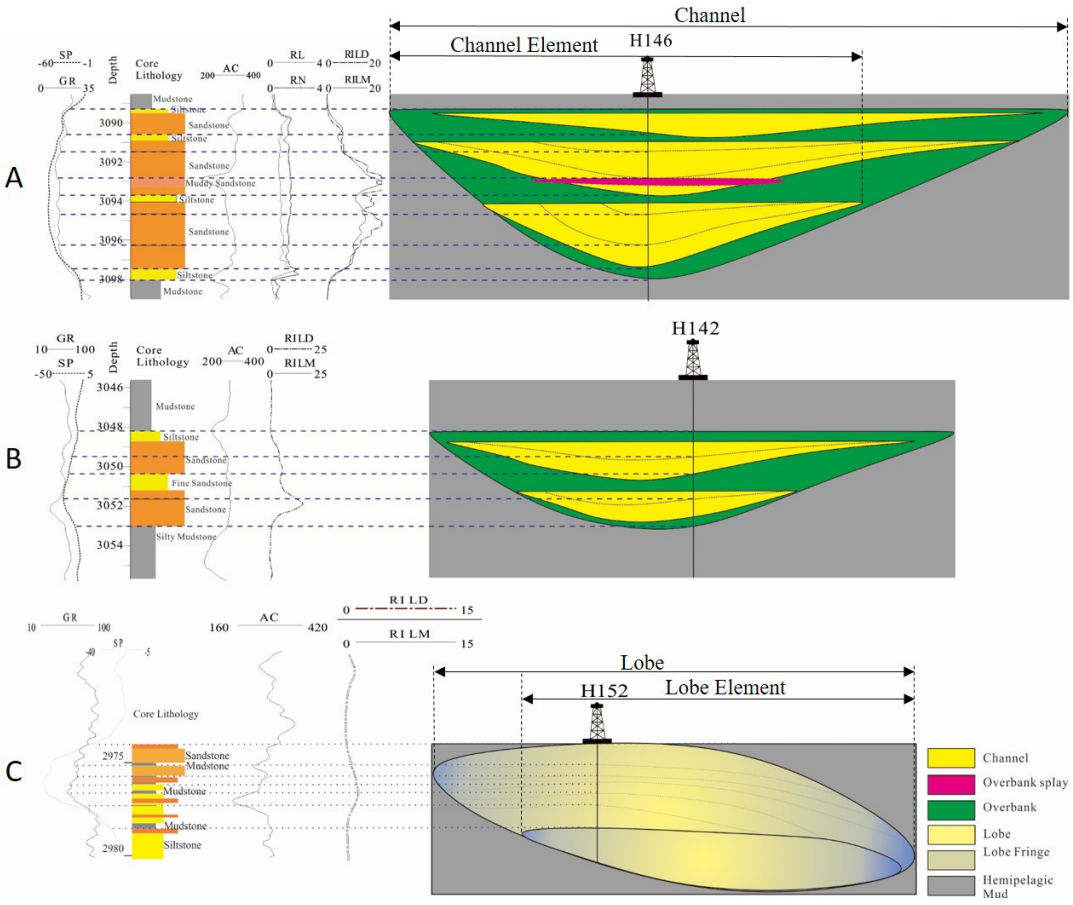

Figure 9: An illustration of channel and lobe elements; (A) bigger channel elements; (B) smaller channel elements; (C) lobe elements. Note; interpretation is made with the help of core lithology and log motifs.

long-term breaks in sedimentation. These units are equivalent to the "second-order" depositional stage of Mutti and Normark [56]. The target stratigraphic interval in the study area is bounded by these surfaces at both its top and bottom (Figure 10). These surfaces exhibit a regional extent and are well documented throughout the basin.

4.4 Sequence stratigraphy

The highly organized nature of turbidite deposits reflects their controls over the development of stratal architecture through a set of well-governed laws [19]. The relative position of the shoreline to the shelf edge, which is controlled by the physiography and accommodation of the shelf, is key. The feeder system dynamically controls the amount and grain size of the sediments that are delivered to deep-water settings [11, 79]. The controlling factors in lacustrine basins are different, as continuous rifting controls the accommodation and slope angle. Due to the smaller size of the lacustrine basin and its intensive degree of extension, frequent sequence cycles developed in Es3m. Thus, a scheme similar to that of Sprague *et al.* [77] is adopted here to depict the sequence stratigraphic framework of Es3m in the study area. A sequence hierarchy is developed based on the interpretations of the main facies types and their lateral and vertical distributions. A sequence (S) comprises a sand-rich lowstand that is capped by transgressive and highstand hemipelagic mudstones. Systematically stacked sequences form composite sequences (CS) that can be further grouped into composite sequence sets (CSS); refer to Sprague *et al.* [77] for further details. Sequences exhibit predictable stacking patterns and can be stacked into composite sequences that comprise a lowstand sequence set and a transgressive and highstand sequence set. A total of forty-five sequences comprising four composite sequences are identified in one composite sequence set. Starting from the bottom and moving towards the top, the four composite sequences are CS4, CS3, CS2 and CS1 (Figure 11).

CS1 is mainly composed of channels and splays that mostly comprise massive sand facies. The channel sand

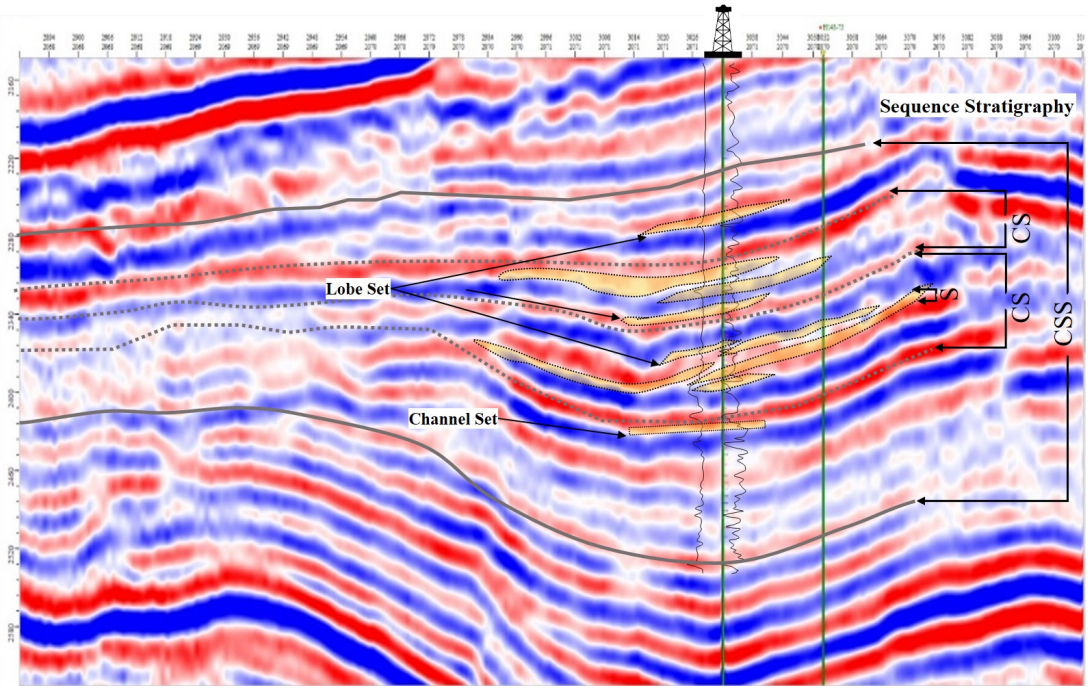

Figure 10: Seismic-section through the study area showing recognition of 4th, 5th, 6th and 7th order surfaces from seismic profile. Location of this section C-C' can be seen in figure 2.

bodies exhibit good connectivity. These sequences are stacked in a progradational pattern, in which lowstand channels prograde basinward over highstand and transgressive hemipelagic mudstones and siltstones. From CS1 to CS2, the channel switches to sequences of thick lobes. In CS2, sequences are also stacked in a progradational pattern, where lowstand lobe sands step basinward over highstand and transgressive hemipelagic mudstones and siltstones. CS3 is dominated by thin lobe fringe bodies, where sequences are stacked in retrogradational patterns in which lowstand lobe fringe sands step backwards towards land and highstand and transgressive mudstones and siltstones onlap onto lobe facies. CS4 is also retrogradational and is dominated by lobes and lobe fringes. In this composite sequence, lobes grade to lobe fringes laterally basinward. CS1 and CS2 reflect high-energy proximal settings, whereas CS3 and CS4 are relatively distal.

The systematic development of turbidite sequences can be related to changes in sea level [59]. Based on the thicknesses of regionally mappable hemipelagic mudstone, a hierarchy can be established from deep-water systems [5, 29, 32, 63, 64]. The Es3m turbidites developed while intense extension occurred in a nearly E–W-trending rift basin. Channels developed on the slopes during the cutting stage, and mixed clastic flows in the channels eroded the substrate; in contrast, stacked lobes that record no significant evidence of erosion represent the fill stage (Figure 11). Extensive channel complexes developed in sequence four. Variations in the flow and/or sediment loads of the channels changed their paths and patterns. Overall, the channels in the study area largely record evidence of lateral accretion and bifurcation. The plan-view map shows that the channels originated from the eastern side of the study area (Figure 12D), while the shifting locations of lobes indicate the presence of multiple feeders (Figure 12A, B, C). Typically, lobes developed during later sequences; for example, the lobes in sequence 2 are progradational, whereas those in sequences 3 and 4 are retrogradational.

4.5 Reservoir Quality

4.5.1 Mineralogy

Rock composition represents a critical parameter that can be used to understand reservoir producibility and water flooding, as it can provide valuable insights into the wettability and saturation of the reservoir [75]. The sandstones in this study are generally lithic arkose but range in composition from arkose to feldspathic litharenite. The average composition of the framework grains is $Q_{45}F_{34}L_{21}$. As a major constituent mineral, quartz represents 35% to 55% of the framework grains. Feldspar is the second most abundant mineral and ranges in abundance from

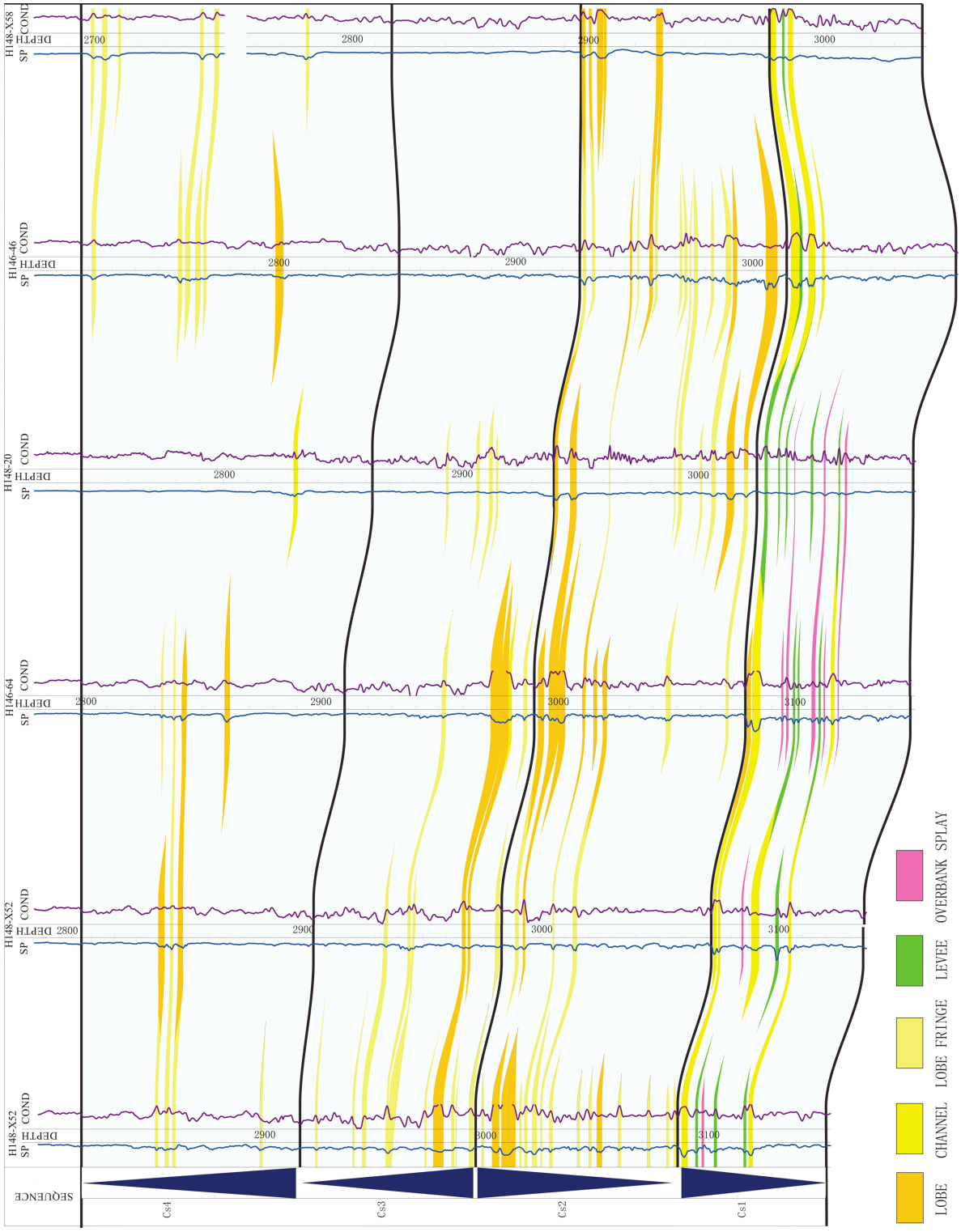

Figure 11: NW-NE cross-section covering study area passing through six wells: Channel developed in CS1 by prograding pattern; thick lobes developed in CS2 by prograding pattern while thin lobes and lobe fringes developed in CS3 and CS4 by retrograding pattern. (See location of cross-section F-F' in Figure 2).

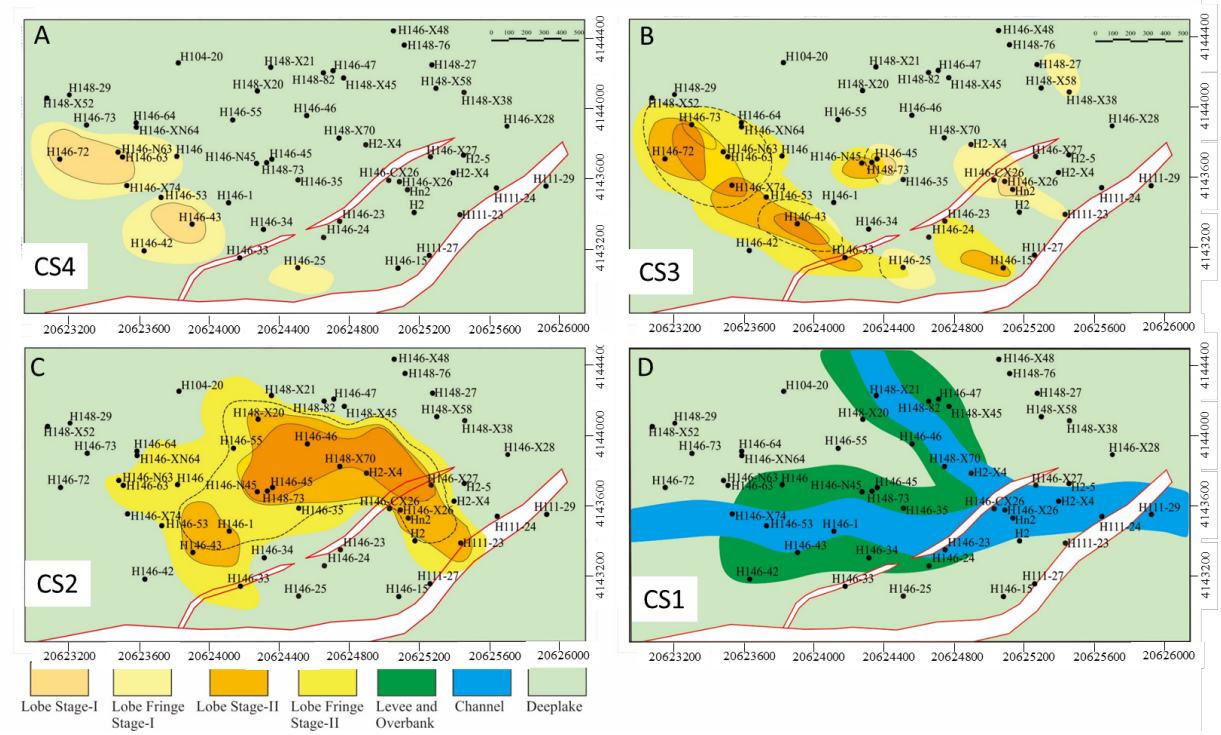

Figure 12: Map showing architectural elements mapped in plain view representing end stage of each composite sequences (A) CS4, shows retrogradational pattern of architectural elements; (B) CS3, also shows retrogradational pattern; (C) CS2, shows progradational pattern of architectural elements; (D) CS1, shows progradational pattern. Maps are based on inferred information from spatial and temporal references gathered from multiple data sets of study area.

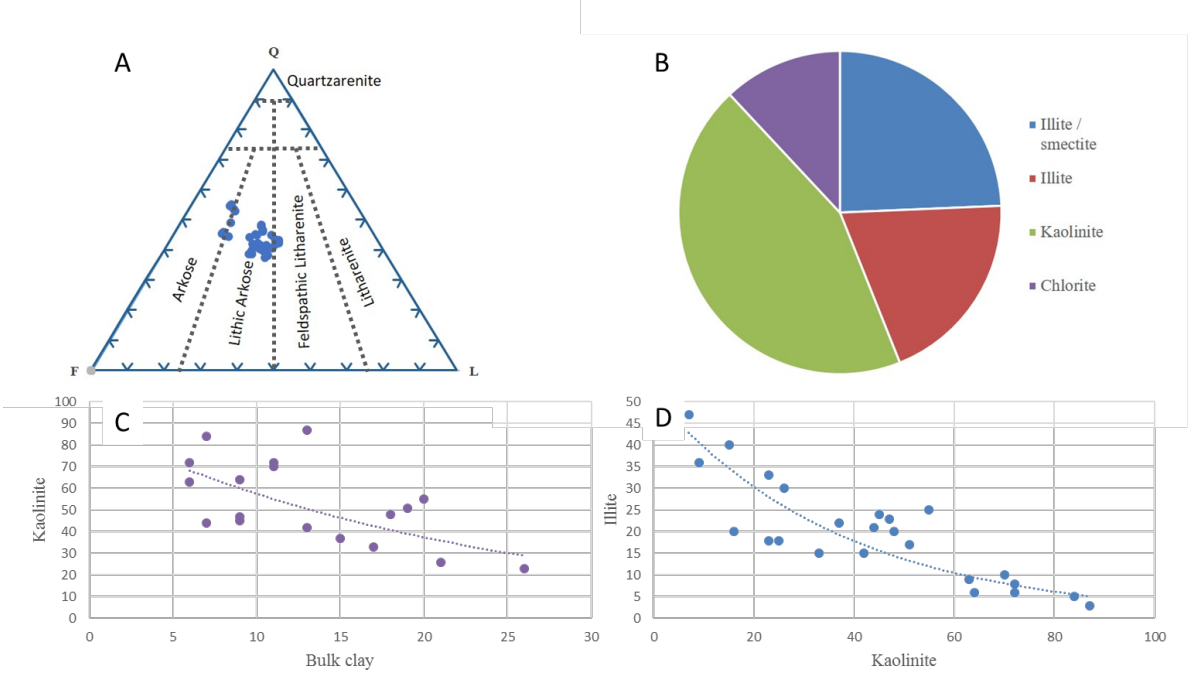

Figure 13: (A) Trinary diagram showing framework grain composition of ES_3m turbidite sandstone from the study area. Diagram refers to sandstone classification standard of Folk *et al.* [20]; (B) Relative weight percent of different clay mineral found in ES_3m sandstone by XRD analysis, kaolinite weighs major part of clay fraction; (C) Graph showing negative relation between bulk clay content and kaolinite content; (D) Negative relation between kaolinite content and illite content.

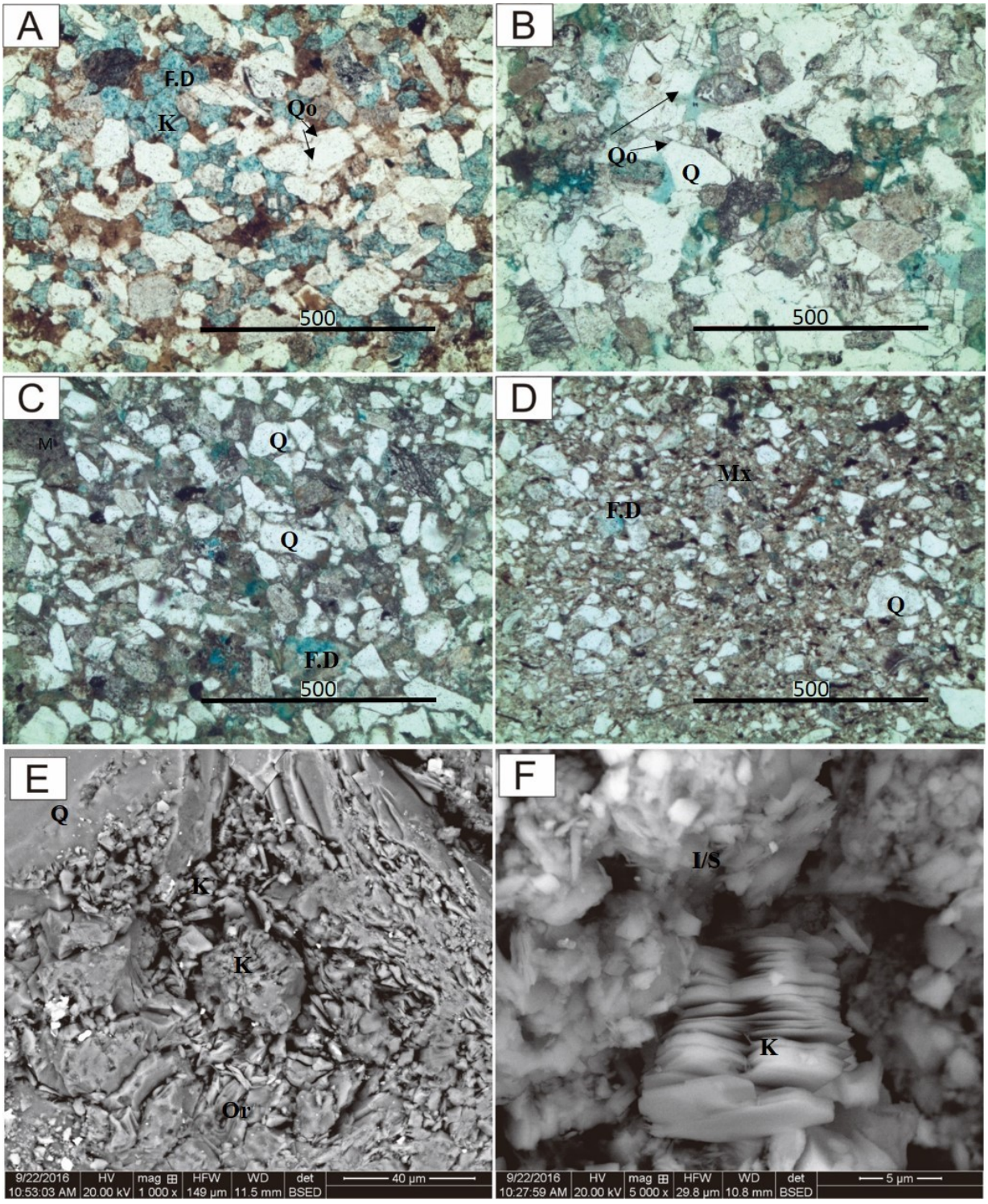

Figure 14: Thin-section photographs showing petrographic features of different architectural elements (A) Channel axis, High intergranular porosity, dissolved feldspar grain; (B) Levee or relative low intergranular porosity; quartz cement is prominent; (C) Lobe Axis, smaller grain size, relatively higher lithic content and less intergranular porosity; (D) Lobe Fringe, higher clay matrix, smaller grain size, very less porosity; (E) Authigenic kaolinite in dissolved Feldspar grain (Orthoclase); (F) Platy crystal structure in kaolinite and fibrous structure in illite-smectite mix layer. F.D-Dissoluted Feldspar, M-Mud intraclasts, Mx- Matrix, Q-Quartz, Qo-Quartz overgrowth, K-Kaolinite; I/S- illite/smectite mixed layer.

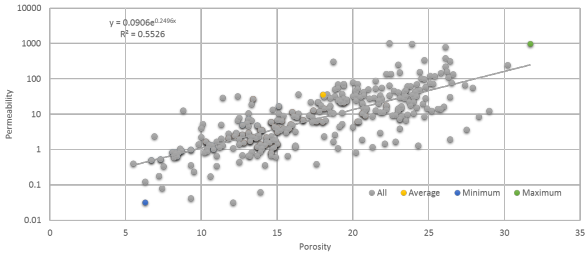

Figure 15: Plot showing overall relationship between porosity and permeability in the study area.

26% to 41%, whereas the fraction of lithic fragments varies from 10% to 24%. The relative fractions of quartz, feldspar and lithic fragments are shown on a ternary diagram (Figure 13A). The lithic fragments are mostly of metamorphic in origin, with very few sedimentary and igneous clasts. Generally, the grain size varies from fine sand to coarse sand. These sandstones are usually poorly to moderately sorted. Their high clay matrix contents and mudclast contents result in their poor sorting. The results of XRD analyses indicate that their bulk clay contents range from 6-26%; the most abundant clays are kaolinite and illite, although chlorite and illite-smectite mixed layers are also present in smaller fractions. Figure 13B shows the relative proportions of these clay minerals. Kaolinite is generally authigenic and is produced by feldspar alteration. Kaolinite content exhibits a negative correlation with total clay content; with increasing total clay, the kaolinite content decreases (and vice versa). Kaolinite also exhibits a negative correlation with illite (Figure 13C, D). These relations indicate that feldspar transformed into kaolinite and that kaolinite transformed into illite. Quartz is mostly monocrystalline, with euhedral edges produced by the formation of quartz overgrowths in channel elements with moderate sorting and relatively large grain sizes (Figure 14A, B). In contrast, lobe elements exhibit finer grain sizes, poor sorting, higher matrix contents and a higher fraction of lithic grains (Figure 14C, D). The dissolution of feldspar is vertically associated with the bed center and spatially associated with the axial areas of channels and lobes. The dissolution of feldspar generated kaolinite, which is present in dissolved pore spaces (Figure 14A, E, F).

4.5.2 Porosity and permeability

The porosity and permeability of the Es3m sandstones and siltstones were measured using routine core analysis. A total of 301 core analysis data points were collected from 9 different wells in the study area (Figure 15). The porosity in Es3m has an average value of 18%, a minimum value of 6.3% and a maximum value of 31.7%. The permeability ranges from 0.032 mD to 992 mD, with an average permeability of 35.83 mD. Primary porosity in the form of intragranular pores is dominant in the Es3m sandstone. However, dissolved and altered feldspar grains can host considerable amounts of secondary porosity (representing 20-50% of the total porosity).

The percolation of meteoric water through pores is responsible for the dissolution of the feldspar. The formation of authigenic kaolinite and illite in secondary pores is due to the release of Al^{3+} and SiO_2 from the leached feldspar [89]. The secondary porosity can reach up to 2% in thin sections. The results of the petrographic analysis of sandstone indicate that increased lithic fragments and clay and silt contents are present in the distal areas of the fan. This led to the poor sorting and lower permeability observed in the study area. Porosity and permeability show good overall relationships in the study area (Figure 15). However, regions of scatter or disruption of their relationships correspond to distal fan areas where considerable microporosity can exist in matrix clay and cement. Due to the small sizes and large pore throat radii of these micropores, their permeability is low.

5 Discussion

Reservoirs have four scales of heterogeneity [46]: 1. microscopic heterogeneity at the pore and throat scale (μm); 2. mesoscopic heterogeneity corresponding to ripple- and cross lamination-scale variability (cm to m); 3. macroscopic heterogeneity reflecting the depositional pattern of lithofacies and subsequent changes after burial (1-100 m); and 4. megascopic heterogeneity corresponding to depositional system-scale variations (1000 m).

Macroscopic heterogeneity is the product of primarily depositional and subsequent diagenetic patterns. Diagenetic calcareous dissolution, accretionary surfaces and small-scale hemipelagic mud capping are responsible for this heterogeneity.

Massive sandstones and clean sand facies were deposited near the channel and lobe axis where turbidity currents were strong, whereas laminated sandstones and siltstones were deposited off-axis, where the currents were weak and dilute [27, 41, 43, 60]. The distributions of facies in channels and lobes do not simply radiate outwards. Massive sands always alternate with clayey deposits off-axis and in turbidite systems. High-energy turbidite flows

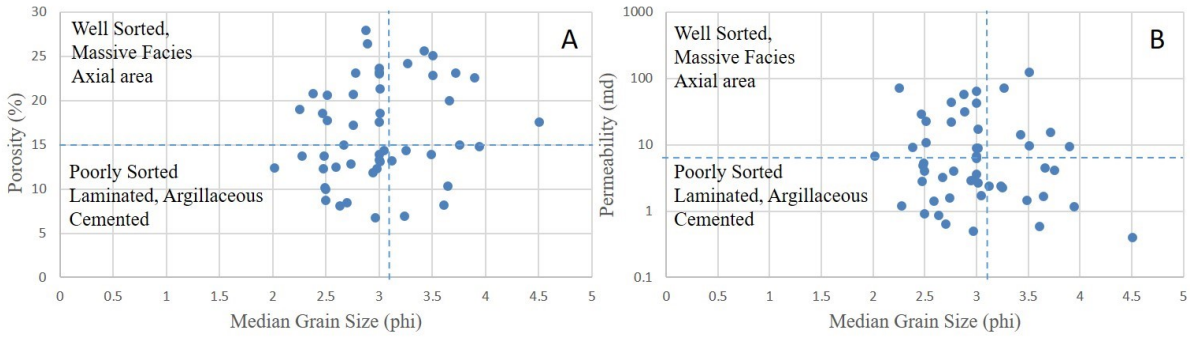

Figure 16: (A) Relationship between median grain size and Porosity; (B) Relationship between median grain size and permeability. Higher Median Grain sizes correspond to higher porosity and permeability in cleaner sandstones while silty, clayed, cemented and laminated sandstones exhibit less porosity and permeability.

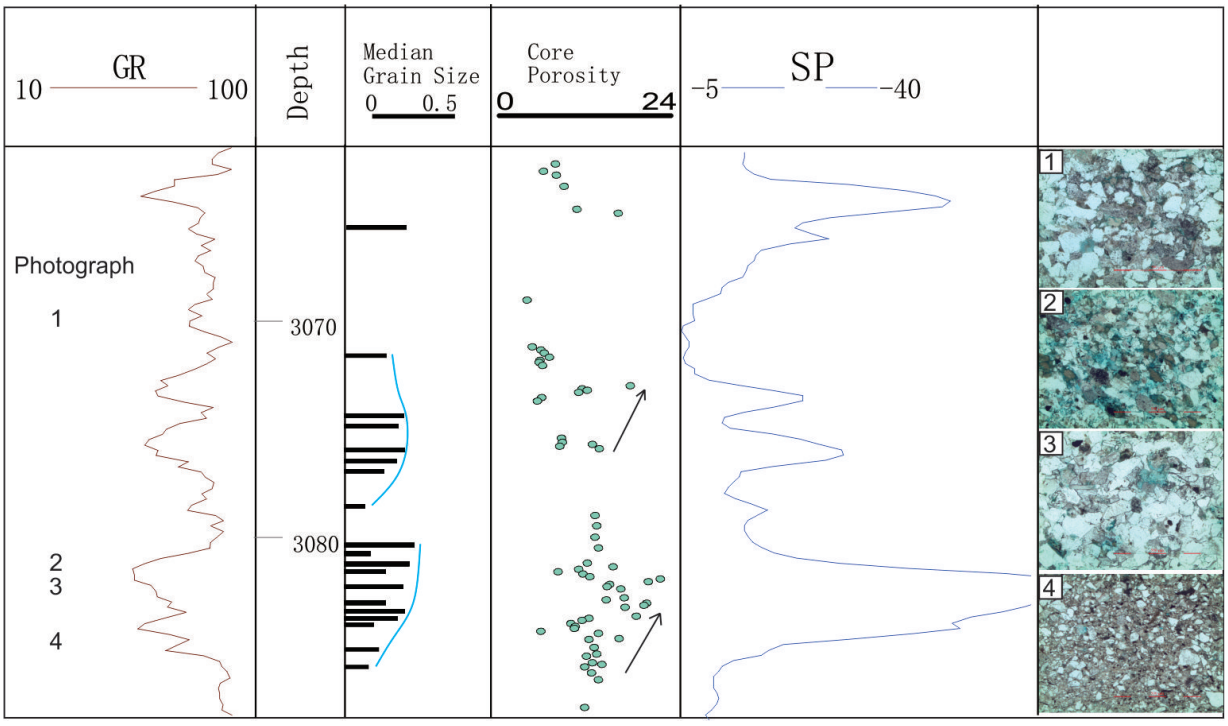

Figure 17: Wireline log (GR and SP), median grain size analyses, routine core analyses and microphotographs from well W152 showing characteristic porosity and grain distribution in vertical profile of lobe. Grain size and porosity increases toward the top of lobe; (Numbers in GR column indicate the depth location of photo microphotographs).

in axial areas maintain a coarser sand supply, producing massive and ripple-laminated facies. Coarser grains in well-sorted facies produce larger pores and throats that ultimately result in higher degrees of porosity and permeability (Figure 16A, B).

The overall architecture depends upon the stacking patterns of macroforms, minor elements and their underlying relief [60]. Analyses of thin sections and core porosity and permeability show that the axial areas of channels and lobes are highly porous and exhibit the higher permeability associated with coarser sandstones (Figure 17). The internal architectural style resulting from a stacking pattern plays a vital role in defining the petrophysical properties of a system. In this system, the progradation of lobes and lateral accretion in channels resulted in the development of coarsening-upward and fining-upward grain size trends (Figure 17). In contrast, splays and distal fan facies display aggradation and exhibit finer grain size fractions with no significant grading. These textural tends are also reflected in their porosity and permeability (Figure 17). This contrasting behavior between different elements produces a composite vertical flow profile.

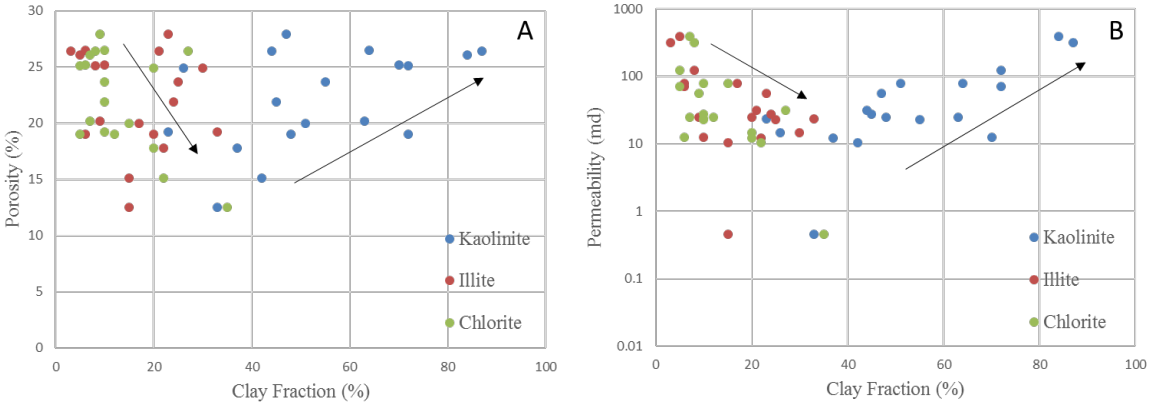

Figure 18: Showing relationship between relative fraction of different clay minerals and core porosity (A) increasing porosity with increasing kaolinite content; (B) increasing permeability with increasing kaolinite content. While porosity and permeability decreases with increasing illite and chlorite content.

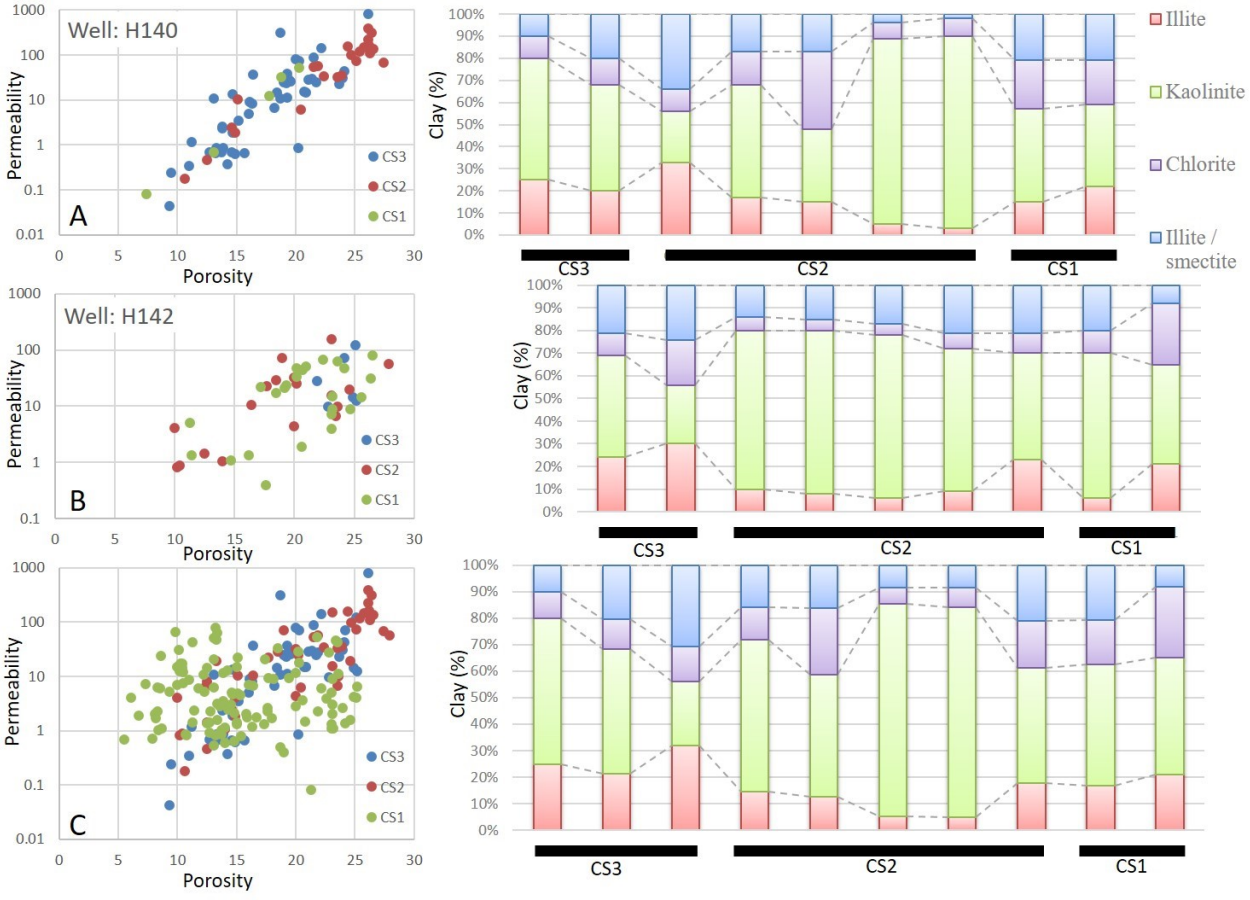

Figure 19: A comparison of poro-perm with clay mineralogy reflects higher content of kaolinite corresponds to higher poro-perm. (A) In well 140, higher content of kaolinite in CS2 corresponds to higher poro-perm; (B) In well 152, higher content of kaolinite in CS2 and CS1 reflected again in higher poro-perm; (C) In Multiple wells, higher content of kaolinite corresponds to higher poro-perm.

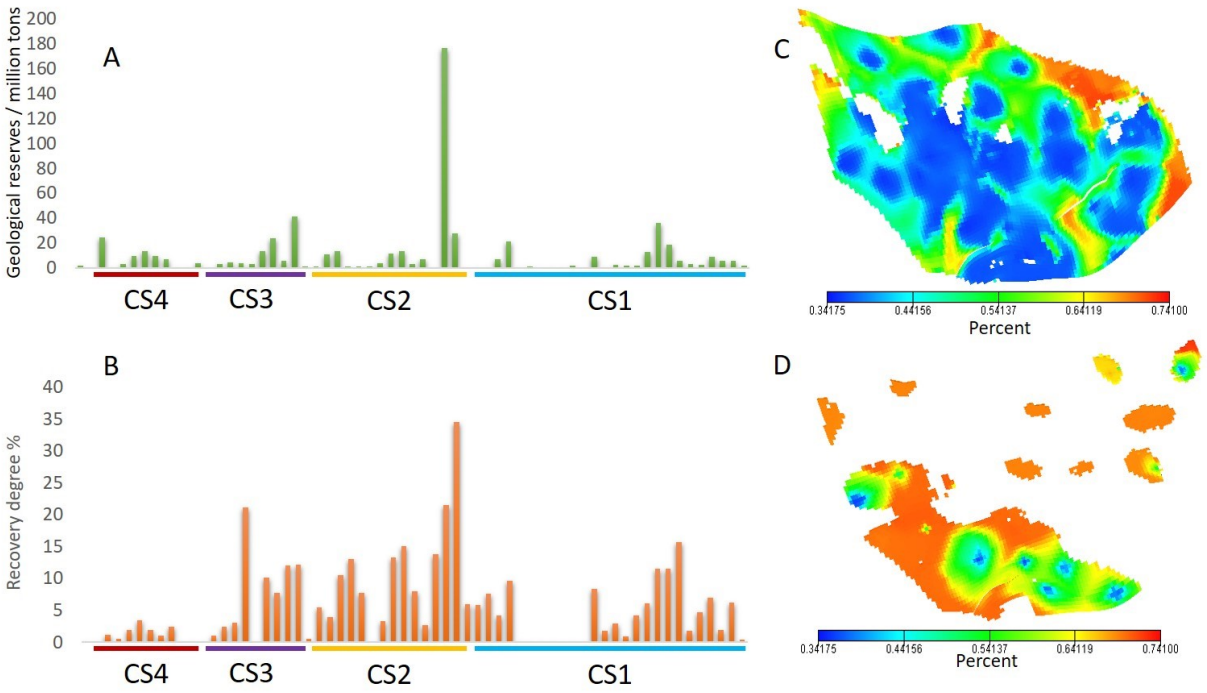

Figure 20: A graphical representation of estimated reserves, recovery rate and remaining oil fractions. (A) estimated oil reserves; (B) Recovery percentage in four composites sequence sets. Map showing remaining oil percentage in (C) CS1 and (D) CS2.

On the microscopic scale, Yuan *et al.* [89] suggested that most likely the internal source for quartz cements in these sandstones is minimal pressure dissolution of feldspars. This dissolution of feldspar produces authigenic clay and quartz cement. This process not only produces secondary microporosity but also destroys primary intergranular pore spaces. This phenomenon produces narrow and occluded pore throats and ultimately reduces permeability. The thicknesses of sandstone beds and their distances from capping mud layers are also factors controlling the pore space and permeability of reservoirs [89]. Secondary porosity associated with feldspar and primary intergranular porosity tend to decrease towards bed margins. In contrast, carbonate cementation tends to increase towards bed margins. Authigenic clays and quartz cement associated with feldspar dissolution tend to occur in the central portions of beds. Microscopic heterogeneity is formed by the combined effects of sedimentary textures and diagenesis. Inherent intergranular pore space and post-burial alteration processes (*i.e.*, cementation, dissolution, and compaction) define the ultimate quality of the reservoir. The dissolution of feldspar grains creates secondary porosity composed of micropores with narrow throats. On the other hand, authigenic clays and quartz cement can occlude intergranular spaces, thereby reducing the overall permeability of the reservoir. Clay is an important component that controls the recovery of the reservoir [68, 78]. The volume of secondary and enhanced production is somewhat proportional to the clay content [80]. Production is also directly proportional to the total clay content [81]. The clay location is also a significant aspect, as grain-rimming and pore-filling clays can drastically increase or decrease the reservoir quality. Previous studies [75, 80, 81] used kaolinite to predict the production and recovery of reservoirs. We determined that higher porosities and permeabilities in the Es3m sandstone are related to higher kaolinite contents (Figure 18A, B). In the context of its sequence stratigraphy, CS2 has the highest kaolinite contents, whereas CS1 and CS3 have lower kaolinite contents (Figure 19A, C). Routine core analyses (Figure 19A, C) show that the overall porosity and permeability are higher in CS2 than they are in the study area.

Well H142 has a high kaolinite content in CS2, which corresponds to its high porosity and permeability, and well H142 exhibits higher porosity and permeability in CS1 than in CS4 due to its higher kaolinite content (Figure 19B). The estimated geological reserves in CS2 are quite high, *i.e.*, approximately 200 million tons (Figure 20A). The recovery percent is also higher in CS2 (Figure 20B, D) than in CS1, which shows a lower recovery percentage (Figure 20C). The remaining oil fractions are lower in the ax-

ial areas of architectural elements, while marginal areas exhibit higher oil fractions (Figure 20C, D).

6 Conclusions

It is necessary to identify the role that reservoir architecture plays in controlling primary, secondary and enhanced production. Previous studies performed in this study area did not address reservoir architecture; therefore, it was difficult to recognize reservoir flow units and their controls on flow. In this study, we identified the reservoir architecture based on the analysis of drill cores, wireline logs and seismic profiles. Five lithofacies were defined according to their deep-water processes and depositional mechanisms. A hierarchy of sequence boundaries was established, and the distribution of architectural elements within these hierarchy levels was also described. The following conclusions can be made from this study:

Massive sandstone facies mainly represent axial areas, while laminated facies represent the marginal areas of lobes and channels, which exhibit high intergranular porosity and good reservoir characteristics. Lobe fringe and channel overbank areas are mainly composed of argillaceous siltstone or fine sandstone with poor reservoir characteristics. High reservoir compartmentalization is formed by transgressive or highstand siltstones or mudstones (SB). These siltstones have low permeability and thus limit fluid flow, especially during secondary production. Sandstone-mudstone interfaces also represent local sites for carbonate cementation. On the other hand, the microporosity that forms in illite, smectite and chlorite generates a pronounced resistance to the permeability of petroleum in the Es3m reservoir. However, higher porosities and permeabilities are associated with higher kaolinite contents. Extensive kaolinization occurs in CS2 and CS1. Lobes in CS2 and channels in CS1 exhibit good reservoir characteristics and considerable connectivity. The channel sand bodies are continuous and have higher recovery rates in axial areas. The lobe sand bodies are small in size and are mostly discontinuous; thus, their recovery rates are lower. Due to the higher degrees of heterogeneity observed at the margins of architectural elements, their remaining oil fractions are also high.

Acknowledgement: The work has been financially supported by the 'China Scholarship Council' and 'National Science and Technology, P.R. China' Project (Special Grant Nos. 2016ZX05027004-002 and 41672129). Special thanks to Geosciences Institute of the Shengli Oilfield, SinoPec, for providing well logs, seismic data and drill cores for the study. Mr. Shizhen Chen and Mr. Zhifeng Sun from the School of Geoscience, China University of Petroleum, are acknowledged for their enormous help with background knowledge and geological context of the area. Professor Jon Gluyas (Durham University) is acknowledged for his valuable reviews and suggestions for improving the quality of the manuscript.

References

[1] Allen, J. R. L., Parallel lamination developed from upper stage plane beds; a model based on the larger coherent structures of the turbulent boundary layer. Sedimentary Geology., 1984, 39(3–4), 227–242. https://doi.org/-

[2] Allen, J. R. L., Studies in fluviatile sedimentation: Bars, bar-complexes and sandstone sheets (low-sinuosity braided streams) in the brownstones (L. devonian), welsh borders. Sedimentary Geology., 1983, 33(4), 237–293. https://doi.org/10.1016/0037-0738(83)90076-3

[3] Amy, L. A., McCaffrey, W. D., & Kneller, B. C., The influence of a lateral basin-slope on the depositional patterns of natural and experimental turbidity currents. Geological Society, London, Special Publications., 2004, 221(1), 311–330. https://doi.org/10.1144/GSL.SP.2004.221.01.17

[4] Amy, L. A., Peachey, S. A., Gardiner, A. A., & Talling, P. J., Prediction of hydrocarbon recovery from turbidite sandstones with linked-debrite facies: Numerical flow-simulation studies. Marine and Petroleum Geology., 2009, 26(10), 2032–2043. https://doi.org/10.1016/j.marpetgeo.2009.02.017

[5] Beaubouef, R. T., Rossen, C., Zelt, F. B., Sullivan, M. D., Mohrig, D. C., & Jennette, G. D. C., Field Guide For AAPG Hedberg Field Research Conference - April 15-20 , Deep-Water Sandstones , Brushy Canyon Formation , West Texas, Field Guide, Am. Assoc. Petrol. Geol., Hedberg Field Research, Conference April 15-20,. In Field Guide For AAPG Hedberg Field Research Conference - April 15-20, 1999 (p. 18). west texas.

[6] Bjørlykke, K., Relationships between depositional environments, burial history and rock properties. Some principal aspects of diagenetic process in sedimentary basins. Sedimentary Geology., 2014, 301, 1–14. https://doi.org/10.1016/j.sedgeo.2013.12.002

[7] Bouma, A. H. A., Fine-grained, mud-rich turbidite systems: model and comparison with coarse-grained, sand-rich systems. Special Publication-Sepm., 2000, 9–19. https://doi.org/10.1144/GSL.SP.2004.222.01.02

[8] Bouma, A. H., Sedimentary characteristics of samples collected from some submarine canyons. Marine Geology., 1965, 3(4), 291–320. https://doi.org/10.1016/0025-3227(65)90040-X

[9] Bridge, J. S., & Diemer, J. A., Quantitative interpretation of an evolving ancient river system. Sedimentology., 1983, 30(5), 599–623. https://doi.org/10.1111/j.1365-3091.1983.tb00698.x

[10] Brown, A. R., Interpretation of Three-Dimensional Seismic Data., Interpretation of Three-Dimensional Seismic Data § (2011). Society of Exploration Geophysicists and American Association of Petroleum Geologists. Retrieved from

http://library.seg.org/doi/book/10.1190/1.9781560802884

[11] Catuneanu, O., Abreu, V., Bhattacharya, J. P., Blum, M. D., Dalrymple, R. W., Eriksson, P. G., … Winker, C., Towards the standardization of sequence stratigraphy. Earth-Science Reviews., 2009. https://doi.org/10.1016/j.earscirev.2008.10.003

[12] Chen, D., Pang, X., Jiang, Z., Zeng, J., Qiu, N., & Li, M., Reservoir characteristics and their effects on hydrocarbon accumulation in lacustrine turbidites in the Jiyang Super-depression, Bohai Bay Basin, China. Marine and Petroleum Geology., 2009, 26(2), 149–162. https://doi.org/10.1016/j.marpetgeo.2008.03.003

[13] Chengshan, W., Xiumian, H., Yongjiang, H., Scott, R. W., & Wagreich, M., Overview of Cretaceous oceanic red beds (Corbs); a window on global oceanic and climate change. Special Publication - Society for Sedimentary Geology., 2009, 91, 13–33. Retrieved from http://www.geoscienceworld.org/cgi/georef/georef;3541135002

[14] Clark, J. D., & Pickering, K. T., Architectural elements and growth patterns of submarine channels: Application to hydrocarbon exploration. AAPG Bulletin., 1996, 80(2), 194–221. https://doi.org/10.1306/64ED878C-1724-11D7-8645000102C1865D

[15] Doyle, J. D., & Sweet, M. L., Three-dimensional distribution of lithofacies, bounding surfaces, porosity, and permeability in a fluvial sandstone - Gypsy Sandstone of northern Oklahoma. American Association of Petroleum Geologists Bulletin., 1995. https://doi.org/10.1306/8D2B14BC-171E-11D7-8645000102C1865D

[16] Dutton, S. P., White, C. D., Willis, B. J., & Novakovic, D., Calcite cement distribution and its effect on fluid flow in a deltaic sandstone, Frontier Formation, Wyoming. AAPG Bulletin., 2002, 86(12), 2007–2021. https://doi.org/10.1306/61EEDDE6-173E-11D7-8645000102C1865D

[17] Eggenhuisen, J. T., McCaffrey, W. D., Haughton, P. D. W., Butler, R. W. H., Moore, I., Jarvie, A., & Hakes, W. G., Reconstructing large-scale remobilisation of deep-water deposits and its impact on sand-body architecture from cored wells: The Lower Cretaceous Britannia Sandstone Formation, UK North Sea. Marine and Petroleum Geology., 2010, 27(7), 1595–1615. https://doi.org/10.1016/j.marpetgeo.2010.04.005

[18] Ercilla, G., Alonso, B., Wynn, R. B., & Baraza, J., Turbidity current sediment waves on irregular slopes: Observations from the Orinoco sediment-wave field. Marine Geology., 2002, 192(1–3), 171–187. https://doi.org/10.1016/S0025-3227(02)00554-6

[19] Flint, S. S., Hodgson, D. M., Sprague, A. R., Brunt, R. L., Van der Merwe, W. C., Figueiredo, J., … Kavanagh, J. P., Depositional architecture and sequence stratigraphy of the Karoo basin floor to shelf edge succession, Laingsburg depocentre, South Africa. Marine and Petroleum Geology., 2011, 28(3), 658–674. https://doi.org/10.1016/j.marpetgeo.2010.06.008

[20] Folk, R. L.; Andrews, P. B.; Lewis, D. W., Detrital sedimentary rock classification and nomenclature for use in new zealand. New Zeal. J. Geol. Geophys., 1970, 13, 937–968, doi:10.1080/00288306.1970.10418211.

[21] Gawthorpe, R. L., Hall, M., Sharp, I., & Dreyer, T., Tectonically enhanced forced regressions: examples from growth folds in extensional and compressional settings, the Miocene of the Suez rift and the Eocene of the Pyrenees. Sedimentary Responses to Forced Regressions., 2000, (June 2007), 177–191. https://doi.org/10.1144/GSL.SP.2000.172.01.09

[22] Gawthorpe, R. L., & Leeder, M. R., Tectono-sedimentary evolution of active extensional basins. Basin Research., 2000, 12(3–4), 195–218. https://doi.org/10.1111/j.1365-2117.2000.00121.x

[23] Gervais, A., Savoye, B., Mulder, T., & Gonthier, E., Sandy modern turbidite lobes: A new insight from high resolution seismic data. Marine and Petroleum Geology., 2006, 23(4), 485–502. https://doi.org/10.1016/j.marpetgeo.2005.10.006

[24] Ghibaudo, G., Subaqueous sediment gravity flow deposits: practical criteria for their field description and classification. Sedimentology., 1992, 39(3), 423–454. https://doi.org/10.1111/j.1365-3091.1992.tb02126.x

[25] Guo, X., He, S., Liu, K., Song, G., Wang, X., & Shi, Z., Oil generation as the dominant overpressure mechanism in the Cenozoic Dongying depression, Bohai Bay Basin, China. AAPG Bulletin., 2010, 94(12), 1859–1881. https://doi.org/10.1306/05191009179

[26] Guo, X.; Liu, K.; He, S.; Song, G.; Wang, Y.; Hao, X.; Wang, B., Petroleum generation and charge history of the northern Dongying Depression, Bohai Bay Basin, China: Insight from integrated fluid inclusion analysis and basin modelling. Mar. Pet. Geol., 2012, 32, 21–35, doi:10.1016/j.marpetgeo.2011.12.007.

[27] Haughton, P., Davis, C., McCaffrey, W., & Barker, S., Hybrid sediment gravity flow deposits - Classification, origin and significance. Marine and Petroleum Geology., 2009, 26(10), 1900–1918. https://doi.org/10.1016/j.marpetgeo.2009.02.012

[28] Henares, S., Caracciolo, L., Cultrone, G., Fernández, J., & Viseras, C., The role of diagenesis and depositional facies on pore system evolution in a Triassic outcrop analogue (SE Spain). Marine and Petroleum Geology., 2014, 51, 136–151. https://doi.org/10.1016/j.marpetgeo.2013.12.004

[29] Hodgson, D. M., Stratigraphic Evolution of Fine-Grained Submarine Fan Systems, Tanqua Depocenter, Karoo Basin, South Africa. Journal of Sedimentary Research., 2006, 76(1), 20–40. https://doi.org/10.2110/jsr.2006.03

[30] Hu, J. Y.; Xu, S. B.; Liu, S. X.; Tong, X., Nonstructural Oil Accumulation; Petroleum Industry Press: Beijing, 1986, 69-221

[31] Jiang, F., Pang, X., Guo, J., Zhou, X., Zhou, X., Liu, D., & Wang, P., Identification and hydrocarbon expulsion history simulation of the effective source rocks in the Dongying Formation, Paleogene, Bohai Sea area, eastern China. Revista Mexicana de Ciencias Geologicas., 2013, 30(2), 355–370.

[32] Johnson, S. D., Flint, S., Hinds, D., & De Ville Wickens, H., Anatomy, geometry and sequence stratigraphy of basin floor to slope turbidite systems, Tanqua Karoo, South Africa. Sedimentology., 2001, 48(5), 987–1023. https://doi.org/10.1046/j.1365-3091.2001.00405.x

[33] Jones, C. M., & McCabe, P. J., Erosion Surfaces Within Giant Fluvial Cross-Beds of the Carboniferous in Northern England. Journal of Sedimentary Research., 1980, Vol. 50(2), 613–620. https://doi.org/10.1306/212F7A63-2B24-11D7-8648000102C1865D

[34] Lampe, C., Song, G., Cong, L., & Mu, X., Fault control on hydrocarbon migration and accumulation in the Tertiary Dongying depression, Bohai Basin, China. AAPG Bulletin., 2012, 96(6), 983–1000. https://doi.org/10.1306/11031109023

[35] Law, S., McDonald, A., Fellows, S., Reed, J., & Sutcliffe, P. G., Influence of Clay Content and Type on Oil Recovery Under Low Salinity Waterflooding in North Sea Reservoirs. SPE Offshore Europe Conference and Exhibition., 2015, (2012). https://doi.org/10.2118/175506-MS

[36] Li Desheng, Geologic evolution of petroliferous basins on continental shelf of china. American Association of Petroleum Geologists Bulletin., 1984.

[37] Li, P. L., Oil/gas distribution patterns in Dongying Depression, Bohai Bay Basin. Journal of Petroleum Science and Engineering., 2004, 41(1–3), 57–66. https://doi.org/10.1016/S0920-4105(03)00143-8

[38] Liu, M., Liu, Z., Sun, X., Wang, B., Zhang, W., & Yao, X., (n.d.) Paleoporosity and critical property in the accumulation period and their impacts on hydrocarbon accumulation — A case study of the middle Es3 member of the Paleogene formation in Niuzhuang Sag, Dongying Depression, Southeastern Bohai Bay Basin, East Ch. In AAPG Annual Convention and Exhibition. Houston, Texas.

[39] Liu, M., Liu, Z., Wang, B., Sun, X., & Guo, J., A new method for recovering paleoporosity of sandstone: case study of middle Es3 member of Paleogene formation in Niuzhuang Sag, Dongying Depression, Bohai Bay Basin in China. Frontiers of Earth Science., 2015, 9(3), 521–530. https://doi.org/10.1007/s11707-015-0493-8

[40] Liu, Q., Zhu, X., Yang, Y., Geng, M., Tan, M., Jiang, L., & Chen, L., Sequence stratigraphy and seismic geomorphology application of facies architecture and sediment-dispersal patterns analysis in the third member of Eocene Shahejie Formation, slope system of Zhanhua Sag, Bohai Bay Basin, China. Marine and Petroleum Geology., 2015, 1–19. https://doi.org/10.1016/j.marpetgeo.2015.11.015

[41] Lowe, D. R., Sediment gravity flows: II Depositional models with special reference to the deposits of high-density turbidity currents. Journal of Sedimentary Petrology., 1982, 52(1), 279–297. https://doi.org/10.1306/212F7F31-2B24-11D7-8648000102C1865D

[42] Lowe, D. R., & Guy, M., Slurry-flow deposits in the Britannia Formation (Lower Cretaceous), North Sea: A new perspective on the turbidity current and debris flow problem. Sedimentology., 2000, 47(1), 31–70. https://doi.org/10.1046/j.1365-3091.2000.00276.x

[43] Mayall, M., Jones, E., & Casey, M., Turbidite channel reservoirs-Key elements in facies prediction and effective development. Marine and Petroleum Geology., 2006, 23(8), 821–841. https://doi.org/10.1016/j.marpetgeo.2006.08.001

[44] McHargue, T., Pyrcz, M. J., Sullivan, M. D., Clark, J. D., Fildani, A., Romans, B. W., … Drinkwater, N. J., Architecture of turbidite channel systems on the continental slope: Patterns and predictions. Marine and Petroleum Geology., 2011, 28(3), 728–743. https://doi.org/10.1016/j.marpetgeo.2010.07.008

[45] Mckee, E. D., & Weir, G. W., Terminology for stratification and cross-stratification in sedimentary rocks. Bulletin of the Geological Society of America., 1953, 64(4), 381–390. https://doi.org/10.1130/0016-7606(1953)64[381:TFSACI]2.0.CO;2

[46] Miall Noel, A. D. T. (Ed.), The Three-Dimensional Facies Architecture of Terrigenous Clastic Sediments and its Implications for Hydrocarbon Discovery and Recovery. SEPM Society for Sedimentary Geology. Retrieved from http://geosciencewo rld.org/content/9781565762268/9781565762268

[47] Miall, A. D., Methods of Architectural-Element Analysis. In The Geology of Fluvial Deposits: Sedimentary Facies, Basin Analysis, and Petroleum Geology (pp. 75–98). Berlin, Heidelberg: Springer Berlin Heidelberg. https://doi.org/10.1007/978-3-662-03237-4_4

[48] Miall, A. D., Reservoir heterogeneities in fluvial sandstones: lesson from outcrop studies. American Association of Petroleum Geologists Bulletin., 1988, 72(6), 682–697. https://doi.org/10.1306/703C8F01-1707-11D7-8645000102C1865D

[49] Miall, A. D., Stratigraphy: A Modern Synthesis. Springer International Publishing Switzerland. https://doi.org/10.1007/978-3-319-24304-7

[50] Miall, A. D., Principles of Sedimentary Basin Analysis (3rd ed.). Springer-Verlag Berlin Heidelberg GmbH. https://doi.org/10.1017/CBO9781107415324.004

[51] Miall, A. D., Architectural elements and bounding surfaces in fluvial deposits: anatomy of the Kayenta formation (lower jurassic), Southwest Colorado. Sedimentary Geology., 1988, 55(3–4). https://doi.org/10.1016/0037-0738(88)90133-9

[52] Middleton, G. V.; Hampton, M. A. Part I. Sediment gravity flows: mechanics of flow and deposition, in G. V. Middleton and A. H. Bouma (eds.); Turbidites and Deep Water Sedimentation; Anaheim, California, 1973, 38

[53] Morad, S.; Al-Ramadan, K.; Ketzer, J. M.; De Ros, L. F., The impact of diagenesis on the heterogeneity of sandstone reservoirs: A review of the role of depositional fades and sequence stratigraphy. Am. Assoc. Pet. Geol. Bull., 2010, 94, 1267–1309.

[54] Munawar, M. J.; Lin, C.; Cnudde, V.; Bultreys, T.; Dong, C.; Zhang, X.; De Boever, W.; Zahid, M. A.; Wu, Y., Petrographic characterization to build an accurate rock model using micro-CT: Case study on low-permeable to tight turbidite sandstone from Eocene Shahejie Formation. Micron, 2018, 109, 22–33, doi:10.1016/j.micron.2018.02.010.

[55] Mutti, E., & Lucchi, F. R., Le torbiditi dell' Appennino settentrionale: introduzione all' analisi di facies. Memoire Geological Society of Italy., 1972, 11, 161–199.

[56] Mutti, E., & Normark, W. R., An Integrated Approach to the Study of Thrbidite Systems. In Seismic Facies and Sedimentary Processes of Submarine Fans and Turbidite Systems (pp. 75–106). Springer-Verlag New York, Inc. https://doi.org/10.1007/978-1-4684-8276-8_4

[57] Mutti, E., Tinterri, R., Benevelli, G., Biase, D. di, & Cavanna, G., Deltaic, mixed and turbidite sedimentation of ancient foreland basins. Marine and Petroleum Geology., 2003, 20(6–8), 733–755. https://doi.org/10.1016/j.marpetgeo.2003.09.001

[58] Pickering, K., Hodgson, D., Platzman, E., Clark, J., & Stephens, C., A new type of bedform produced by backfilling processes in a submarine channel, Late Miocene, Tabernas-Sorbas basin, SE Spain. Journal of Sedimentary Research., 2001, 71(5), 692–704. https://doi.org/10.1306/2DC40960-0E47-11D7-8643000102C1865D

[59] Posamentier, H. W., & Kolla, V., Seismic geomorphology and stratigraphy of depositional elements in deep-water settings. Journal of Sedimentary Research., 2003, 73(3), 367–388. https://doi.org/10.1306/111302730367

[60] Prelat, A., & Hodgson, D. M., The full range of turbidite bed thickness patterns in submarine lobes: controls and implications. Journal of the Geological Society., 2013, 170(1), 209–214. https://doi.org/10.1144/jgs2012-056

[61] Prelat, A., Hodgson, D. M., & Flint, S. S., Evolution, architecture and hierarchy of distributary deep-water deposits: a high-resolution outcrop investigation from the Permian Karoo Basin, South Africa. Sedimentology., 2009, 56(7), 2132–2154.

https://doi.org/10.1111/j.1365-3091.2009.01073.x

[62] Purvis, K., Kao, J., Flanagan, K., Henderson, J., & Duranti, D., Complex reservoir geometries in a deep water clastic sequence, Gryphon Field, UKCS: Injection structures, geological modelling and reservoir simulation. Marine and Petroleum Geology., 2002, 19(2), 161–179. https://doi.org/10.1016/S0264-8172(02)00003-X

[63] Pyles, D. R., Multiscale stratigraphic analysis of a structurally confined submarine fan: Carboniferous Ross Sandstone, Ireland. AAPG Bulletin., 2008, 92(5), 557–587. https://doi.org/10.1306/01110807042

[64] Pyles, D. R., Syvitski, J. P. M., & Slatt, R. M., Defining the concept of stratigraphic grade and applying it to stratal (reservoir) architecture and evolution of the slope-to-basin profile: An outcrop perspective. Marine and Petroleum Geology., 2011, 28(3), 675–697. https://doi.org/10.1016/j.marpetgeo.2010.07.006

[65] Rustichelli, A., Tondi, E., Agosta, F., Di Celma, C., & Giorgioni, M., Sedimentologic and diagenetic controls on pore-network characteristics of Oligocene-Miocene ramp carbonates (Majella Mountain, central Italy). AAPG Bulletin., 2013, 97(3), 487–524. https://doi.org/10.1306/07311212071

[66] Saito, T., & Ito, M., Deposition of sheet-like turbidite packets and migration of channel-overbank systems on a sandy submarine fan: An example from the Late Miocene-Early Pliocene forearc basin, Boso Peninsula, Japan. Sedimentary Geology., 2002, 149(4), 265–277. https://doi.org/10.1016/S0037-0738(01)00179-8

[67] Schwehr, K., Driscoll, N., & Tauxe, L., Origin of continental margin morphology: Submarine-slide or downslope current-controlled bedforms, a rock magnetic approach. Marine Geology., 2007, 240(1–4), 19–41. https://doi.org/10.1016/j.margeo.2007.01.012

[68] Seccombe, J., Lager, A., Jerauld, G., Jhaveri, B., Buikema, T., Bassler, S., … Fueg, E., Demonstration of Low-Salinity EOR at Interwell Scale, Endicott Field, Alaska. SPE Improved Oil Recovery Symposium., 2010, 2008. https://doi.org/10.2118/129692-MS

[69] Shanmugam, G., Types of porosity in sandstones and their significance in interpreting provenance. Provenance of arenites. Proc. Cetraro, Cosenza, 1984. https://doi.org/10.1007/978-94-017-2809-6_6

[70] Shanmugam, G., Ten turbidite myths. Earth-Science Reviews., 2002, 58(3–4), 311–341. https://doi.org/10.1016/S0012-8252(02)00065-X

[71] Shanmugam, G., 50 years of the turbidite paradigm (1950s-1990s): Deep-water processes and facies models-a critical perspective. In Marine and Petroleum Geology (Vol. 17, pp. 285–342). https://doi.org/10.1016/S0264-8172(99)00011-2

[72] Shanmugam, G., Lehtonen, L. R., Straume, T., Syvertsen, S. E., Hodgkinson, R. J., & Skibeli, M., Slump and debris-flow dominated upper slope facies in the Cretaceous of the Norwegian and northern North Seas (61-67°N): implications for sand distribution. American Association of Petroleum Geologists Bulletin., 1994. https://doi.org/-

[73] Shanmugam, G., & Moiola, R. J., Reinterpretation of Depositional Processes in a Classic Flysch Sequence (Pennsylvanian Jackfork Group), Ouachita Mountains, Arkansas and Oklahoma: Discussion. AAPG Bulletin., 1997, 81(3), 672–695. https://doi.org/10.1306/522B43A7-1727-11D7-8645000102C1865D

[74] Shanmugam, G., Spalding, T. D., & Rofheart, D. H., Process Sedimentology and Reservoir Quality of Deep-Marine Bottom-Current Reworked Sands (Sandy Contourites): An Example from the Gulf of Mexico. AAPG Bulletin., 1993, 77(7), 1241–1259. https://doi.org/10.1306/BDFF8E52-1718-11D7-8645000102C1865D

[75] Shehata, A. M., Alotaibi, M. B., & Nasr-El-Din, H. A., Waterflooding in Carbonate Reservoirs : Does the Salinity Matter? SPE Reservoir Evaluation & Engineering., 2014, 17(3), 304–313. https://doi.org/10.2118/170254-PA

[76] Song, G., & Chen, H., Quantitative evaluation of transporting efficiencies for hydrocarbon migration along different unconformities in a Cainozoic lacustrine basin: Examples from the Dongying Depression, Bohai Bay Basin, east China. Journal of Geochemical Exploration., 2009, 101(1), 97. https://doi.org/10.1016/j.gexplo.2008.12.048

[77] Sprague, A. R. G., Sullivan, M. D., Campion, K. M., & Jensen, G. N., The physical stratigraphy of deep-water strata: A hierarchical approach to the analysis of genetically-related stratigraphic elements for improved reservoir prediction. AAPG Annual Meeting, Program with Abstracts., 2002, 11(123), A167–A168. Retrieved from http://scholar.google.com/scholar?hl=en&btnG=Search&q=intitle:The+Physical+Stratigraphy+of+Deep-Water+Strata+:+A+Hierarchical+Approach+to+the+Analysis+of+Genetically+Related+Stratigraphic+Elements+for+Improved+Reservoir+Prediction#0

[78] Suijkerbuijk, B., Hofman, J., Ligthelm, D. J., Romanuka, J., Brussee, N., van der Linde, H., & Marcelis, A. H. M., Fundamental Investigations into Wettability and Low Salinity Flooding by Parameter Isolation. SPE Improved Oil Recovery Symposium., 2013, 1–23. https://doi.org/10.2118/154204-MS

[79] Talling, P. J., How and where do incised valleys form if sea level remains above the shelf edge? Geology., 1998, 26(1), 87–90. https://doi.org/10.1130/0091-7613(1998)026<0087:HAWDIV>2.3.CO

[80] Tang, G. Q., & Morrow, N. R., Salinity, Temperature, Oil Composition, and Oil Recovery by Waterflooding. SPE Reservoir Engineering., 1997, 12(November), 269–276. https://doi.org/10.2118/36680-PA

[81] Thyne, G., Wettability Alteration in Reservoirs: How it Applies to Alaskan Oil Production., the SPE Western Regional Meeting held in Anchorage §(2016). Society of Petroleum Engineers. https://doi.org/10.2118/180370-MS

[82] Tyler, N., & Finley, R. J., Architectural controls on the recovery of hydrocarbons from sandstone reservoirs. In A. D. Miall & N. Tyler (Eds.), The Three-Dimensional Facies Architecture of Terrigenous Clastic Sediments and its Implications for Hydrocarbon Discovery and Recovery (pp. 1–5). SEPM (Society for Sedimentary Geology), Tulsa, OK. https://doi.org/10.2110/csp.91.03

[83] Vakarelov, B. K., & Bruce Ainsworth, R., A hierarchical approach to architectural classification in marginal-marine systems: Bridging the gap between sedimentology and sequence stratigraphy. AAPG Bulletin., 2013, 97(7), 1121–1161. https://doi.org/10.1306/11011212024

[84] Van der Werff, W., & Johnson, S., High resolution stratigraphic analysis of a turbidite system, Tanqua Karoo Basin, South Africa. Marine and Petroleum Geology., 2003, 20(1), 45–69. https://doi.org/10.1016/S0264-8172(03)00025-4

[85] Wang, C.; Hu, X.; huang, Y.; scott, R. W.; wagreich, M., Overview of Cretaceous Oceanic Red Beds (CORBs): A Window on Global

Oceanic and Climate Change. In Cretaceous Ocean Redbeds., 2009, 13–33 ISBN 978-1-56576-135-3.

[86] Xu, J. W. Lateral shifting of the Tanlu Fault and its geological significance. In Proceedings of the Symposium of International Exchanges for Earth Sciences; 1980, 129– 142.

[87] Yuan, G., Cao, Y., Cluyas, J., Li, X., Xi, K., Wang, Y., ... Oxtoby, N. H., Feldspar dissolution, authigenic clays, and quartz cements in open and closed sandstone geochemical systems during diagenesis: Typical examples from two sags in Bohai Bay Basin, East China. AAPG Bulletin., 2015, 99(11), 2121–2154. https://doi.org/10.1306/07101514004

[88] Yuan, G., Cao, Y., Cluyas, J., Li, X., Xi, K., Wang, Y., ... Oxtoby, N. H., Feldspar dissolution, authigenic clays, and quartz cements in open and closed sandstone geochemical systems during diagenesis: Typical examples from two sags in Bohai Bay Basin, East China. AAPG Bulletin., 2015, 99(11), 2121–2154. https://doi.org/10.1306/07101514004

[89] Yuan, G., Gluyas, J., Cao, Y., Oxtoby, N. H., Jia, Z., Wang, Y., ... Li, X., Diagenesis and reservoir quality evolution of the Eocene sandstones in the northern Dongying Sag, Bohai Bay Basin, East China. Marine and Petroleum Geology., 2015, 62, 77–89. https://doi.org/10.1016/j.marpetgeo.2015.01.006

[90] Zahid, M. A.; Chunmei, D.; Lin, C.; Gluyas, J.; Jones, S.; Zhang, X.; Munawar, M. J.; Ma, C. Sequence stratigraphy, sedimentary facies and reservoir quality of Es4s, southern slope of Dongying Depression, Bohai Bay Basin, East China. Mar. Pet. Geol., 2016, 77, 448–470, doi:10.1016/j.marpetgeo.2016.06.026.

[91] Zhang, L., Liu, Q., Zhu, R., Li, Z., & Lu, X., Source rocks in Mesozoic-Cenozoic continental rift basins, east China: A case from Dongying Depression, Bohai Bay Basin. Organic Geochemistry., 2009, 40(2), 229–242. https://doi.org/10.1016/j.orggeochem.2008.10.013

[92] Zhang, S. W., The application of an integrated approach in exploration of lacustrine turbidites in Jiyang Sub-basin, Bohai Bay Basin, China. Journal of Petroleum Science and Engineering., 2004, 41(1–3), 67–77. https://doi.org/10.1016/S0920-4105(03)00144-X

[93] Zhang, T., Zhang, X., Lin, C., Yu, J., & Zhang, S., Seismic sedimentology interpretation method of meandering fluvial reservoir: From model to real data. Journal of Earth Science., 2015, 26(4), 598–606. https://doi.org/10.1007/s12583-015-0572-5

[94] Zhang, X., Lin, C., & Zhang, T., Seismic sedimentology and its application in shallow sea area, gentle slope belt of Chengning uplift. Journal of Earth Science., 2010, 21(4), 471–479. https://doi.org/10.1007/s12583-010-0108-y